1982

Synthesis and characterization of oxide interstitial derivatives of zirconium monochloride and monobromide

Linda Mae Seaverson
Iowa State University

Seaverson, Linda Mae

SYNTHESIS AND CHARACTERIZATION OF OXIDE INTERSTITIAL DERIVATIVES OF ZIRCONIUM MONOCHLORIDE AND MONOBROMIDE

Iowa State University PH.D. 1982

Synthesis and characterization of oxide interstitial derivatives of zirconium monochloride and monobromide

by

Linda Mae Seaverson

A Dissertation Submitted to the
Graduate Faculty in Partial Fulfillment of the
Requirements for the Degree of
DOCTOR OF PHILOSOPHY

Department: Chemistry
Major: Inorganic Chemistry

Approved:

Signature was redacted for privacy.

In Charge of Major Work

Signature was redacted for privacy.

For the Major Department

Signature was redacted for privacy.

For the Graduate College

Iowa State University
Ames, Iowa

1982

TABLE OF CONTENTS

INTRODUCTION

Investigations into the synthesis and characterization of reduced binary and ternary zirconium halides have produced what is becoming a lengthy list of new compounds with fascinating structures and physical properties. Two fine representatives of this list are the zirconium monohalides, ZrCl and ZrBr. The present work is concerned with the further understanding of their reactivity. This introduction will acquaint the reader with what is known of their synthesis, structure, and reactivity, and elaborate on the primary interests of the present work.

Synthesis of ZrX

In 1970, Struss and Corbett[1] reported the monochloride as a co-product of a hot-cold reaction containing metal at the hot (600°C*) end and $ZrCl_4$ in a middle region of a sealed tantalum container. After twelve days, the metal had a 2-3 mil layer of gray metallic product ($ZrCl + ZrCl_2$) which was covered with a trace of a brown layer. $ZrCl_2$ was found in the middle region and $ZrCl_3$ was found at the cool (500°) end. When they equilibrated the gray metallic mixture with a ten-fold excess of Zr foil for about five days at 625°, quantitative conversion to ZrCl resulted. Equilibration at 525° was found to be inadequate. Their Debye-Scherrer x-ray powder pattern data indicated a homogeneity range on the high chloride side with Cl:Zr ≥ 1.14 at 675°. They also

*All temperatures will be reported in centigrade.

reported ZrCl disproportionated to Zr and $ZrCl_4$ at an observable rate under high vacuum at 610°. The ZrCl was analyzed by helium-fusion (in graphite) and found to contain 0.6% oxygen, 0.04% nitrogen, and no hydrogen.

In the same year, Troyanov and Tsirel'nikov[2] reported their preparation of ZrCl. Zirconium foil inside a Mo tube was placed at one end of a fused silica tube. A temperature gradient of 900° at one end and 600° at the other end (900°/600°)* was imposed along the foil. The cool end of the fused silica was 330°. They estimated this produced a $ZrCl_4$ vapor pressure of approximately 1 atm. After 4.3 days, the foil in the 750-800° region had completely reacted while the rest was relatively untouched. They described the monochloride as shiny black plates which were quite stable in air, requiring two months for a crystal to completely decompose, and relatively inert in water but dissolving in weak acids. They reported it as trigonal with rhombohedral cell parameters of $\underline{a}$ = 9.12 ± 0.01Å, α = 21.62 ± 0.08 and Z = 2.

Both of the above papers make reference to a material produced and patented by Dean[3,4] under the name "Zirklor" consisting of 25-28% Cl and the rest Zr (ZrCl is 28% Cl and 72% Zr). This was produced by electrolytic reduction of an $SrCl_2$-NaCl-$ZrCl_4$ melt (63:34:3) on graphite. The powder pattern was very different from those found by both Struss and Corbett[1] and Troyanov and Tsirel'nikov[2] which agreed with each other

---

*All temperature gradients will be reported as T_2/T_1 where T_2 and T_1 represent the end temperatures of the object specified (i.e., foil, Ta tube).

except for the absence of the weak d = 9.73 Å line by the latter. Struss and Corbett[1] obtained a sample of "Zirklor" and found it to be poorly crystalline but to have essentially the ZrCl pattern.

Zirconium monobromide preparation was first reported by Troyanov et al.[5] in 1973. They used the same synthetic technique as described above. For 10 1/2 days, a temperature gradient along the Zr metal of 900°/470° was imposed. The cool end of the fused silica was ~335°. As with ZrCl, ZrBr was discovered on the metal only in the 820°/670° region. Also, like ZrCl, the ZrBr was described as soft, reflective, hexagonal plates with similar stability. Trigonal lattice constants of $\underline{a}$ = 3.507 ± 0.001 and $\underline{c}$ = 28.06 ± 0.01 Å with Z = 6 were reported.

Structure of ZrX

In 1973, Troyanov[6] published his structure study of ZrCl based on film data of a single crystal. He concluded the space group was $R\bar{3}m$ with the zirconium and chlorine ions in alternate double layers, a structure without precedent. This structure was solved on the basis of a hexagonal cell with lattice constants $\underline{a}$ = 3.41 and $\underline{c}$ = 26.74 Å and 60 h0ℓ reflections. The resulting poor refinement (R = 0.29) was blamed on inaccurate measurement of their intensities. From his interlayer Zr-Zr distance (2.87 Å), he concluded the presence of metal-metal bonding. Other interatomic distances were 3.41 Å for intralayer Zr-Zr or Cl-Cl, 2.81 Å for interlayer Cl-Cl, and 3.10 Å for interlayer Zr-Cl.

In 1976, Adolphson and Corbett[7] improved on Troyanov's findings with a single crystal study using integrated diffractometer data.

Although they first refined (R = 0.080, R_w = 0.087) the structure as monoclinic, space group C2, with lattice parameters $\underline{a}$ = 5.943(6), $\underline{b}$ = 3.419, $\underline{c}$ = 9.087(18) Å, β = 102.5(1), and Z = 4, further study revealed better refinement (R = 0.071, R_w = 0.087) as trigonal, $R\bar{3}m$ with lattice parameters $\underline{a}$ = 3.424(2) and $\underline{c}$ = 26.57(4) Å, and Z = 6. Daake and Corbett[8] later improved these lattice constants, $\underline{a}$ = 3.4233(5) and $\underline{c}$ = 26.693 Å, with the use of Guinier camera data. Adolphson and Corbett verified the structure consisted of cubic close packed zirconium and chlorine atoms in alternate double layers in the form of Cl-Zr-Zr-Cl slabs. The cubic close packing of the layers requires three Cl-Zr-Zr-Cl slabs for a repeat and thus the large $\underline{c}$ parameter. Their refinement yielded more reasonable interatomic distances than Troyanov's. The Zr-Zr and Cl-Cl intralayer distances were 3.424(2) Å, Zr-Zr interlayer distance was 3.087(5) Å, Cl-Cl interlayer distance was 3.607(14) Å. The short Zr-Zr interlayer distance, 0.10 Å less than in the metal, led them to predict strong metal-metal bonding also. The Cl-Cl interlayer distance, the interslab distance, was consistent with a van der Waals gap.

Troyanov et al.[5] predicted from the powder pattern data that ZrBr belonged to the trigonal $R\bar{3}m$ space group and was isostructural with ZrCl. Daake and Corbett[8] were able to refine (R = 0.16) the structure from Guinier powder pattern data in a hexagonal cell with lattice dimensions $\underline{a}$ = 3.5031(3) and $\underline{c}$ = 28.071(3) Å. They noticed the ZrBr powder pattern contained more and sharper reflections with different intensities than ZrCl. Furthermore, powder patterns of ZrBr were less

susceptible to broadening due to grinding damage of the sample. Their solution found the structure of ZrBr to also contain X-Zr-Zr-X slabs but with an alternate stacking sequence of the slabs. Whereas the slabs stack ABCA in ZrCl, they stack ACBA in ZrBr. Thus, while the interlayer coordination is trigonal antiprismatic about the chlorine in ZrCl (three metals and three halogens), it is trigonal prismatic about the bromine in ZrBr. The metal has trigonal antiprismatic coordination to adjacent halide and metal layers in both structures. The ZrBr case allows the Zr to "see" halide through interstices, whereas the ZrCl does not. This, Daake and Corbett[8] explain, causes the greater strength, fewer stacking defects and lesser susceptibility to grinding damage of ZrBr.

These structures have a graphitic-like nature and high melting point (>1100°)[8]. Band calculations of Marchiando et al.[9] predicted very strong bonds within the four layer slabs, consistent with high melting temperature, and weak bonds between slabs to the extent that the bonding may be van der Waals type, consistent with the graphitic-like nature. This bonding scheme also explains the anisotropic electrical conductivities normal to (10^{-3} ohm^{-1} cm^{-1}) vs within (10^{2} ohm^{-1} cm^{-1}) the layers.[2,5] Their calculations predicted a nonzero density of states at the Fermi level with the band made up of mostly Zr-4d orbitals. Daake and Corbett[8] reported the room temperature magnetic susceptibility as Pauli paramagnetic, appropriate for a metallic compound with the indicated Zr-Cl density at the Fermi level.

Reactivity of ZrX

The structural and physical characteristics of the zirconium monohalides described above make them essentially two-dimensional metals with infinite double metal layers. These characteristics make them candidates for interesting reactions and subsequent products. Research in this area has included synthesis of other reduced halides, attempts at intercalation between the halide layers, synthesis of hydrides, and a brief look at reaction with ZrO_2. This work is briefly reviewed below.

The zirconium monohalides provide a more reactive reductant than the pure metal. Daake and Corbett[10] were able to synthesize high purity anhydrous trihalides with tetrahalide and monohalide without the intermediate products or unreacted metal typical after reaction of tetrahalide with metal. Corbett et al.[11] further report the synthesis of transported 3R-$ZrCl_2$ from the reaction of ZrCl and $ZrCl_3$ at 650°/750° for approximately one month and transported Zr_6Cl_{15}, the first cluster ion of transition group IV, under similar conditions.

The similarity of these structures to the transition metal sulfides which intercalate so easily[12,13] led Daake and Corbett[8] to suspect similar results might be obtained for the zirconium monohalides. However, they found no detectable changes in the lattice parameters. Liquid pyridine with both ZrCl and ZrBr, liquid NH_3 with ZrBr, liquid N_2H_4 with ZrBr, liquid triphenylphosphine with ZrBr, gaseous Al_2Cl_6 with ZrCl, and I_2 in CCl_4 with ZrCl were attempted.

Reversible hydrogenation of ZrCl and ZrBr was reported by Struss

and Corbett[14] in 1977. Slightly nonstoichiometric hemi- and monohydrides were prepared with the hemihydrides being darker gray than the parent halides and the monohalides being brass for ZrClH and bronze for ZrBrH. Even at room temperature, ZrX absorbs hydrogen at ~1 Torr/s with 1 atm. pressure.

Recently, Marek et al.[15] have reported their structure results derived from powder pattern data of $ZrBrH_{0.5}$, ZrBrH, and ZrClH. For the monohydrides, the zirconium and halide layers stacking sequence changed from abca (ZrX) of the $R\bar{3}m$ space group to abab of the $P\bar{3}m1$ space group. Best results for $ZrBrH_{0.5}$ were obtained in space group C2/m, a subgroup of $R\bar{3}m$, with a distorted one slab variation of the ZrBr structure with zig-zag chains of distorted metal tetrahedra parallel to lattice dimension b. Centers of shared tetrahedra are considered too close for simultaneous occupancy so the authors believed the hemihydride stoichiometry is achieved by alternate zig-zag chain occupancy as predicted by the NMR studies of Hwang et al.[16] The absence of order due to defects, as suggested by neutron diffraction data,[17] resulted in crystallographically indistinguishable chains.

Daake[18] reported increased lattice dimensions of 2% in a and 1% in c for ZrCl and 1.76% in a and 1.45% in c for ZrBr after reaction with 0.33 mole fraction of ZrO_2 at 850° for eight days. He believed the expansion was caused by the removal of electron density from between the zirconium layers as a result of the substitution of the oxide for the halide ions, $ZrX_{1-n}O_n$ (X = Cl, Br).

Present Work

The present work attempted to successfully intercalate ZrCl and investigated the reaction of ZrX with ZrO_2. The latter emphasized the determination of reaction saturation and reversibility, a structure analysis of the oxidized ZrX, the collection of ESCA data on approximately saturated ZrCl, the discovery and limited study of the transport capability of oxidized ZrX, an attempt to find analogous phases with other anions, and a study of the oxidized Zr coproduct.

EXPERIMENTAL

Synthesis Techniques

General

The air and moisture sensitivity of the reactants and products required transfers and manipulations to be performed with dry box and vacuum techniques. The dry boxes were constantly purged with dry N_2 which recirculated through a column of Molecular Sieve. This and a tray of P_2O_5 in the dry boxes typically reduced the H_2O atmosphere to 1-4 ppm. Pyrex vacuum lines equipped with Hg diffusion pumps were available for evacuation of sample tubes, dynamic vacuum sublimation, and hydrogenation.

Tantalum containers (0.95 cm o.d.) in fused silica jackets[19,20] were employed to contain the reactions. No reaction between Ta and ZrO_2 was assured since $4\ Ta + 5\ ZrO_2 \rightarrow 5\ Zr + 2\ Ta_2O_5$ has $\Delta H^\circ_{298} = 226.0$ kcal mole^{-1} and $\Delta G^\circ_{298} = 212.4$ kcal mole^{-1} according to data from NBS.[21] Chromel-alumel thermocouples attached on the outside of the jacket at the extremes of the Ta tubes monitored their temperatures.

Reactants

Reactor-grade zirconium metal (<500 ppm Hf) strips were prepared and cleaned as described by Guthrie.[19] Zirconium turnings, 3-4 mil thick, were obtained from Rich Schmidt's group. They were cleaned first with Skelly B to remove grease and then conc. HCl to remove iron. Zirconium powder was prepared by first hydrogenating Zr strips at 450-500° for seven hours, grinding the embrittled metal with an agate mortar

and pestle, and lastly dehydrogenating by slowly heating in high vacuum from 300° to 800°. The lattice constants of the resulting Zr powder are within 1σ of those of oxygen-free Zr.[22]

Most $ZrCl_4$ used was prepared by reaction of electronic-grade HCl with Zr strips at 300° for 5 hrs and was sublimed over a generous amount of metal and ZrCl at 370-400° for 6 hrs to remove any $FeCl_3$. $ZrCl_4$ was also purchased from Aldrich and likewise sublimed. All $ZrCl_4$ samples contained <200 ppm Hf. $ZrBr_4$ with <<0.1% Hf was prepared by reaction of bromine and zirconium turnings in a four zone evaculated and sealed fused silica vessel and was sublimed in another three zone fused silica vessel under vacuum.

Most of the zirconium monohalides used were prepared by either Dr. R. L. Daake or Dr. H. Imoto by the method developed by Daake.[18] New supplies were prepared by the same technique. In one case, a mixture of reduced bromides prepared by Daake was used instead of $ZrBr_4$. Although Daake[18] reported 99.5% yields of ZrX with maximum temperatures of 825° for both ZrCl and ZrBr preparations, the present work found this temperature only gave high purity yields for ZrCl. In addition to ZrBr, it yielded ~15% $ZrBr_3$ and unreacted Zr turnings. A maximum temperature of 795° was found to produce high purity yields.

The ZrO_2 was prepared by Schweiter[23] by passing an air stream over $ZrOCl_2 \cdot 8\ H_2O$ at either 600° for 1 hr, 300-350° for 4 hr, or 350° for 6 hr. It was analyzed to contain <200 ppm Hf. No hydroxyl peak appeared in the infrared spectrum of a nujol mull. Unfortunately, after all data were collected, the ZrO_2 was discovered to be slightly contaminated

with chloride. X-ray fluorescence found 1.9 ± 0.4% Cl (by weight) after calibration with standards or a molar ratio of Cl:Zr = 0.07 ± 0.01. Spectrophotometric analysis after heating in NaOH found 0.37 ± 0.001% (by weight) soluble chloride or a molar ratio of Cl:Zr = 0.016 ± 0.004. In any case, this material will be referred to as "ZrO_2" throughout this dissertation.

ZrN and ZrC were purchased from Cerac, Inc. Both samples were analyzed to contain <200 ppm Hf. Each was degassed at 250° under dynamic vacuum in an open Ta tube for 24 hours. The ZrF_4 used was prepared by Fukutomi and Corbett.[24] It was twice sublimed in a Ta jacket at 600°. Emission spectroscopy found no impurities other than a trace of iron and titanium. $ZrS_{0.867}$ (WC-type ZrS), $ZrS_{1.29}$ (NaCl-type ZrS) and ZrS_2 were obtained from Dr. H. Franzen and co-workers. The preparation of these materials has been described by Conrad and Franzen.[25,26]

Reactions

Details of the intercalation experiments will be reported on a per case basis in the RESULTS section.

Desired masses of ZrX and ZrO_2 (ZrN, ZrS_y, ZrF_4, or ZrC) and sometimes Zr powder generally totaling less than 300 mg., were weighed in separate glass vials, ground together, and enclosed in a Ta tube. The majority of reactions were heated at 1000° for two weeks with little temperature gradient along the tube.

Normally reactions were cooled by shutting off the furnace, allowing the temperature to fall to ambient. When reactions were cooled 1-4°/hr, a motorized potentiometer was attached to the controller's

thermocouple. Transport reactions of $ZrX(O_y)$ were performed in 18 cm long Ta tubes with one end a short distance out of the tube furnace to accomplish the temperature gradient ~950°/~500°. Further details of these reactions will be reported as needed in the RESULTS section.

Characterization Techniques

General

Most elemental analyses were performed by Edward DeKalb by emission spectroscopy, x-ray fluorescence spectroscopy; or, in the case of Hf analyses, by spectral analysis of a graphite pellet subjected to a spark. Francis C. Laabs conducted electron microprobe examinations with an ARL-model EMX instrument using a focused beam at 19.7 Kv and a specimen current of 2 namp.

Photoelectron spectra, both XPS (Al K_α = 1486.6 eV) and UPS (He I = 21.21 eV), were obtained on a AEI Model ES200B instrument coupled to a Nicolet 1180 microcomputer. Three to thirteen scans were collected per examination using 512 channels with a monochromator in use for the XPS. No charging was noted. Samples were pressed into an In strip or adhesive tape in the attached drybox (H_2O and O_2 <1 ppm). The instrument was operated by James Anderegg.

The Guinier powder pattern technique was by far the most extensively used analytical method. Details of its use and advantages have been described elsewhere.[18,27] Inaccurate intensities caused by preferred orientation presented no problem here as previous patterns of the monohalides could be used as standards. No reaction with the cellophane

tape was detected. The sample remained unoxidized by air with minimized transfer times.

The reflection positions were measured in millimeters via an imprinted scale (IRDAB Model-750 scaling device) or a Nonius Guinier viewer. Cell dimensions were determined from these measurements as described by Araujo.[28] When calculated powder patterns were desired, either the Yvon et al.[29] or Clark et al.[30] programs were used.

As a first check for successful reaction, the Guinier powder patterns of the products were visually compared with a standard Guinier powder pattern of ZrX. If no noticeable shift in the reflection positions or change in their intensities or addition of new reflections resulted, the extent of reaction was considered so minimal that it could be considered unsuccessful and the lattice dimensions were not determined. Ford[31] has found with even the small amount of Li in $Li_{0.16}YCl$, shifting of YCl reflections can be seen visually. For ZrCl, the 110 and 113 reflections are particularly sensitive to changes in the lattice dimensions.

Single crystal work

Three crystal structures of $ZrCl(O_y)$ were resolved: $ZrCl(O_{0.25})$, $ZrCl(O_{0.29})$, and $ZrCl(O_{0.43})$. The first stoichiometry resulted from the first single crystal found of this phase. It elucidated the location of the oxygen but did not contain the maximum amount of oxygen. For this reason, the third crystal structure study was undertaken. The second, $ZrCl(O_{0.29})$, was initiated because the compound was believed to

contain sulfur instead of oxygen but electron microprobe analysis later found no sulfur. One $ZrBr(O_y)$ structure, $ZrBr(O_{0.29})$, was attempted with limited success.

Single crystals were found by first opening the Ta tube in a drybox equipped with a microscope. Selected crystals were inserted into 0.3 mm glass capillaries which were temporarily sealed with petroleum jelly. Once outside the drybox, they were sealed with a gas flame and the ends were covered with Apiezon W. Oscillation, and zero- and first-level (HOℓ) Weissenberg photographs (Charles Supper Co. camera) established their singularity and strong diffracting ability, and the absence of superstructure spots.

The data sets were collected using either the Datex or Ames Laboratory diffractometers[32,33] which were interfaced to a PDP-15 computer and equipped with Mo K_α radiation (λ = 0.70926 Å) monochromatized by a graphite single crystal. The intensities of three standard reflections were monitored every 75 reflections to check for instrument and crystal stability. Never did evidence of decay appear. Four octants of data were collected with no restrictions. Final lattice dimensions were obtained by a least squares fit of reflections ($25° < 2\theta < 40°$) which were tuned for both Friedel-related peaks. Observed reflections ($I > 3\sigma(I)$) were corrected for Lorentz-polarization effects[34] and their standard deviations[35] were calculated as usual. Examination of the data sets always revealed that the systematic extinction condition $-h+k+\ell = 3n$ applied and $R\bar{3}m$ (No. 166), the space group of ZrCl, was chosen. An empirical absorption correction was carried out using

diffractometer ϕ-scan data, tuning on each peak, and the program TALABS[36] or ABSN[37] (μ = 64.9 cm^{-1} for $ZrCl(O_y)$, μ = 251 cm^{-1} for $ZrBr(O_y)$[38]). Averaging with FDATA[39] yielded the independent data set with no reflections ever eliminated at a cutoff of 6σ. Structure factor calculations and least squares refinement were done using the full matrix program ALLS.[17] Fourier series calculations were done using the program FOUR[40] and for molecular drawings the program ORTEP[41] was used. Calculations on the $ZrCl(O_{0.43(2)})$ structure were carried out on a VAX 11/780 computer. The others were carried out with the Berkeley computer or at the Iowa State University computation center. Table I compiles the data collection details for the four structures.

Knudsen cell mass spectrometry

The cell was a 2.5 cm long, 0.6 cm o.d. Ta tube with one end closed by a welded cap. The cap covering the other end was sometimes welded and had a 4-13 mil orifice. The smaller orifices were prepared by Mr. Gary Wells by denting a cap with a special punch and sanding until an opening appeared. The instrument used was equipped with a boron nitride furnace with a resistive heating element built by James Anderegg and a Universal Voltronics Corp. voltage supply which allowed heating up to 1000 ± 4°. Temperatures were measured with a chromel alumel thermocouple and a voltmeter. An Electronic Associates Inc. Quadrupole Mass Spectrometer Analyzer was used as a detector. The instrument was operated by Anderegg.

Table 1. Data collection details for $ZrCl(O_y)$ and $ZrBr(O_y)$ crystal structures

	$ZrCl(O_y)$			$ZrBr(O_y)$
y =	0.25	0.29	0.43	
Size (mm)	0.16 x 0.14 x 0.005	0.16 x 0.14 x 0.005	0.16 x 0.14 x 0.005	0.16 x 0.14 x 0.10
Octants	HKL, $H\bar{K}L$, $\bar{H}\bar{K}L$, $\bar{H}K\bar{L}$	HKL, $\bar{H}\bar{K}L$, $\bar{H}K\bar{L}$, $H\bar{K}\bar{L}$	HKL, $\bar{H}\bar{K}L$, $\bar{H}\bar{K}L$, $H\bar{K}\bar{L}$	HKL, $\bar{H}\bar{K}L$, $\bar{H}K\bar{L}$, $H\bar{K}\bar{L}$
2θ maximum (deg)	50	50	60	50
Phi-scan reflection (hkℓ, 2θ(deg))	$\bar{2}3\bar{5}$, 37.03	$\bar{1}23$, 23.89	$\bar{2}10$, 23.14	240, 46.70
Reflections Checked	1360	1316	2213	1616
Observed	446	426	723	533
Independent	86	86	141	102
R (ave)	0.053	0.022	0.041	0.033

RESULTS

Intercalation

Ammonia gas attempts involved placing a sample of ZrCl into a quartz pail which easily slipped into and out of a stainless steel tube. Exposure to 10 atm. of undried gas for three days showed no change in the ZrCl Guinier powder pattern. Five days of 8-9 atm. at 300° yielded a darker gray sample with a brass surface and a white coating on the walls of the tube. The Guinier powder pattern showed evidence of $ZrClH_{0.5}$ (dark gray). The gold was suspected then to be $ZrClH_{1.0}$. The coating was suspected to be NH_4Cl or $ZrCl_4$. A third experiment was an attempt to find a temperature which promotes intercalation without hydrogenation. A single sample was subjected to successive overnight 10 atm. exposures at the approximate temperatures of 100°, 130°, 160°, 210°, 260°, and 388°. Reweighing after each exposure found no change until after 388°. However, again the inside of the tube was coated white. The Guinier powder pattern contained NH_4Cl lines and one broad line at d = 1.78 Å which could be a shifted 110 reflection (normally d = 1.75 Å) of ZrCl. The latter suggests an expanded intercalated lattice. The broad line does not correspond to a reflection of $ZrClH_{0.5}$ or ZrClH.

The pyridine attempts involved placing monohalide into a quartz basket and vacuum sealing this together with the dried pyridine in a pyrex tube. This was immersed into a 190° oil bath for two days. After this, a white amorphous-looking material lay on top of a dark solid with

yellow-colored pyridine above it. NMR identified the liquid as pyridine with a minute amount of unknown material. The Guinier powder pattern of the solids showed again some $ZrClH_{0.5}$ but mostly ZrCl without changes.

A $CO_{(g)}$ attempt was tried because it had no possibility of hydride formation. A sample of ZrCl was subjected to 68 atm. of $CO_{(g)}$ at 170°C for 12 hr in a high pressure bomb. Visual and Guinier powder pattern analysis found ZrCl unchanged. No CO peak in the IR of the KBr pellet was seen.

The first n-butyl Li intercalation trial was attempted as described by Dines.[42] A sample of ZrCl on a sintered glass frit was immersed in 0.26 M n-butyl Li in hexane at room temperature for five days in an Ar flushed drybox. Determination of remaining Li in solution by titration as described by Dines proved unsuccessful owing to precipitation and evaporation. The Guinier powder patterns of the products of two attempts showed no deviations from the ZrCl pattern. A high temperature trial involved containing some ZrCl with 1.6 M n-butyl Li in hexane in an evacuated, sealed Pyrex sample tube. This was kept in an oil bath at 50° overnight and 60° for five days. Afterwards, a white precipitate lay on top of the black ZrCl. The solids were washed several times with hexane. The Guinier powder pattern showed only ZrCl without changes.

Dissolved alkali metal in liquid ammonia is another intercalation technique reported in the literature.[43] A sample of Li metal was dissolved in ~10 ml of NH_3 and poured over an equimolar quantity of ZrCl. This was kept at -78° overnight, then -33° for 10 hr, then -78° overnight. The solution did not lose its blue color. A Guinier powder

pattern showed no deviation from that of ZrCl. Under the same conditions, analogous results occurred with potassium in ammonia.

The following alkali metal attempts were performed in Ta tube containers. The reaction, LiCl + $xsZr_{strip}$ + $ZrCl_4$, was an attempt to synthesize ZrCl in the presence of a Li source. It was heated nine days at 700°/618°. Cooling was accomplished by shutting off the furnace. No tube bulging occurred. The strip was chewed up and embrittled from ZrCl formation. Powder patterns showed only unchanged ZrCl and LiCl as products. A second attempt, LiCl + ZrCl + $xsZr_{strip}$, was heated for eight days at 736°/722° and cooled slowly to well below the melting point of LiCl (614°) after which the furnace was shut off. Again, only LiCl and unchanged ZrCl were found on the Guinier powder pattern.

A similar attempt, but with CsCl, was heated for eleven days at 780°/670°. Some pinkish microcrystals were found at the cool end and black crystals were found on the strip. The Guinier powder patterns of the pink crystals showed only CsCl while that of the black was unchanged ZrCl.

To test a higher temperature, the reaction $ZrCl_4$ + 6 Zr_{powder} + 3 NaCl was performed. The heating schedule began at 400° for one day with an increase in temperature of 50° per day to 930°/938°. The Ta tube was found slightly bulged. Only a dark microcrystalline clump, hardened by white NaCl, was found at the original reactants end. The Guinier powder pattern showed an unchanged ZrCl pattern, a shifted Zr pattern which is probably from oxygen impurity, and a NaCl pattern.

A molten alkali metal approach involved the reaction ZrCl + Li in a Ta tube. This reaction was loaded in an Ar-filled drybox to prevent formation of LiN. This was heated to 850° for one day and cooled by shutting off the furnace. Only soft sticky plates were found whose Guinier powder pattern showed an unshifted Zr pattern and four reflections which have not been identified but are unlike Li, LiOH, LiCl, or any $ZrCl_x$. Perhaps an alloy formed but both Ta and Zr have only ppm level solubilities in Li at 850°. The reaction, ZrCl + Li + LiCl, was tried at 550°/540° with the Ta tube in an upright position so that the molten Li would cover the solids. A Guinier powder pattern found ZrCl unchanged, LiCl, perhaps Li, and a few extra lines.

Reaction of ZrX with ZrO_2

General reactions

The heating histories of the various reactions are listed in Tables 2 and 3. The Ta tube containers were very bulged after all reactions. A typical crimped end was rounded out to almost the original 0.95 cm diameter. This corresponds to 30-40 atm. pressure.[18]

Products of the reactions appeared as microcrystalline powders or sintered clumps which were dark gray to very dark olive for the chloride and bronze for the monobromide. As the oxide concentration approached saturation, larger hexagonal plates (0.16 x 0.14 x 0.005 mm) were found. It was discovered that when reactions were cooled by shutting off a furnace with a larger mass (Lindberg furnace) and therefore a slower cool down, the crystals approached singularity. In the three attempts of cooling the furnace at 1-4°/hr from 1000°, many single crystals were

Table 2. Heating histories and trigonal cell dimensions of $ZrCl(O_y)$ phases from general $ZrCl + nZrO_2$ reactions

n	a (Å)	c (Å)	N[a]	Source[b]	Heating history
0[c]	3.4233(5)	26.693(3)	10	G	40.0°-1 day, inc. 50°/day to 825°-1 wk., air quench[d]
0[e]	3.423(5)	26.65(7)	6	G	Same as above
0.08	3.4542(7)	26.797(13)	9	G	481°/953°-2 wk
0.11	3.4623(8)	26.902(11)	10	G	895°/890°-2 wk
0.20	3.4829(5)	26.992(7)	14	G	400°-1 day, inc. 100°/day to 1025°/1016°-10 days
0.22	3.4814(5)	26.973(9)	13	G	1001°/989°-2 wk
0.23	3.4807(6)	26.981(9)	13	G	1016°/1002°-6 days
0.25	3.4920(5)	27.026(8)	10	G	Same as n = 0.20
0.26	3.4940(5)	27.0602(9)	16	G	1000°-2 wk
0.33	3.4905(5)	27.050(9)	14	G	400°, inc. ~100°/day to 1029°/1000°-2 wk
0.43	3.4955(4)	27.032(11)	9	G	Same as n = 0.33
0.67(I)	3.4960(6)	27.049(9)	11	G	Same as n = 0.33
0.67(II)	3.4984(2)	27.065(4)	9	L	Start 300°, inc. 1°/hr. to 1001°/969°-13 days
	3.4993(5)	27.079(10)	10	G	Cooled 1°/hr. to 350°, shut off furnace

[a]Number of indexed reflections used in refinement.
[b]G = Guinier powder pattern data; L = tuned reflections on diffractometer data (LATT).
[c]Reference 8. Annealed sample after grinding.
[d]Unless otherwise stated,the reaction was cooled by only shutting off the furnace.
[e]Sample not annealed after grinding.

Table 3. Heating histories and trigonal cell dimensions of $ZrBr(O_y)$ phases from general $ZrBr + nZrO_2$ reactions

n	a (Å)	c (Å)	N[a]	Source[b]	Heating history
0[c]	3.5031(3)	28.071(3)	23	G	400°-1 day, inc. 50°/day to 795-2 wks., air quench[d]
0	3.5064(2)	28.068(2)	29	G	Same as above
0.11	3.5402(2)	28.313(3)	28	G	890°-4 wks.
0.13	3.5517(2)	28.384(5)	21	G	941°-2 wks.
0.15	3.5594(4)	28.418(5)	13	L	1000°-2 wks., cooled 4°/hr to 25°
	3.5541(3)	28.412(4)	28	G	Same as n = 0.13
0.18	3.5561(2)	28.419(4)	22	G	Same as n = 0.13
0.23	3.5581(3)	28.434(4)	25	G	413°/411°-1 day, inc. 1°/hr to 1007°/1003°-2 wks., cooled 1°/hr to
0.67	3.5587(3)	28.425(6)	22	G	502°/491°

[a-d]Same as Table 2, respectively.

obtained in two monochloride and one monobromide reactions ($ZrClO_{0.25}$, $ZrClO_{0.43}$, and $ZrBr(O_y)$, see Structure results). A more reasonable intermediate cooling rate would probably work also.

Guinier powder patterns of the products showed a shifted ZrX pattern ($ZrX(O_y)$) with no intensity changes but with the typically broad lines sharpened (so lattice dimension accuracy improved), a shifted α-Zr pattern with unchanged intensities, and, at saturation, a monoclinic ZrO_2 pattern. The above can be expressed with the general reaction:

$$ZrX + n\ ZrO_2 \rightarrow v\ ZrX(O_y) + w\ Zr(O_x) \ .$$

The latter product will be referred to as the Zr coproduct.

Tables 2 and 3 list the trigonal cell dimensions of the $ZrCl(O_y)$ and $ZrBr(O_y)$ phases, respectively, for various values of n (moles of ZrO_2 per mole ZrX). Figures 1 and 2 show $\underline{a}$ and $\underline{c}$, respectively, vs. n for the $ZrCl(O_y)$ system. Figures 3 and 4 show $\underline{a}$ and $\underline{c}$, respectively, vs. n for the $ZrBr(O_y)$ system. Tables 4 and 5 list the cell dimensions of the Zr coproduct from the chloride and bromide reactions, respectively. Figures 5 and 6 show the variations of the $\underline{a}$ and $\underline{c}$ dimensions with n.

The average lattice constants of the above phases at saturation, their increases over the parent halides, and n at saturation for both halide systems are listed in Table 6. Best fit lines on both $\underline{a}$ and $\underline{c}$ variations (Figures 1 and 2) predicted saturation at n = 0.27 ± 0.01 mole for $ZrCl(O_y)$. For $ZrBr(O_y)$, Figure 3 predicted n = 0.23 ± 0.01 mole according to the $\underline{a}$ variation and n = 0.21 ± 0.01 mole according to

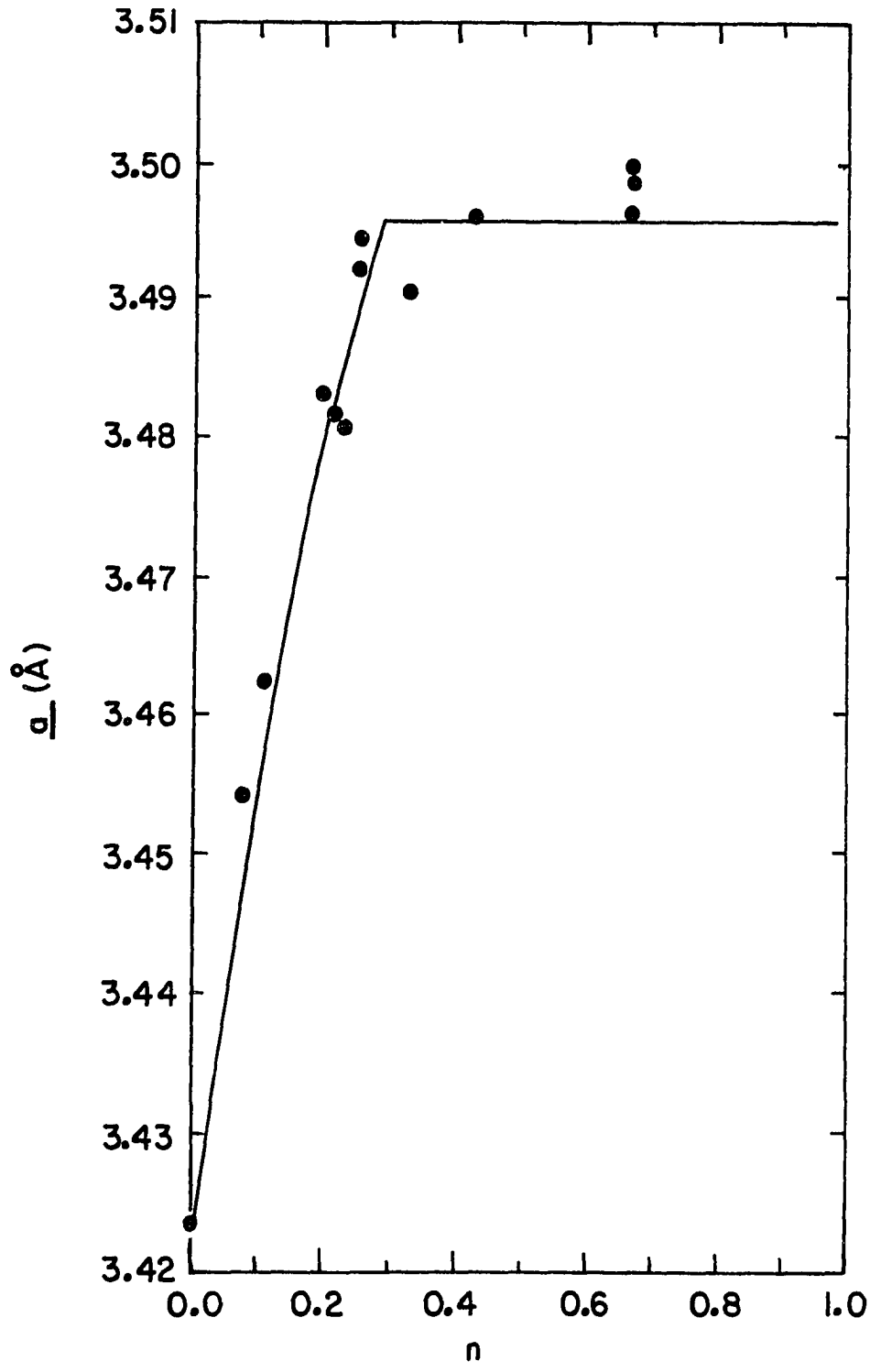

Figure 1. The a cell dimension of $ZrCl(O_y)$ vs. n from ZrCl + n ZrO_2 reactions

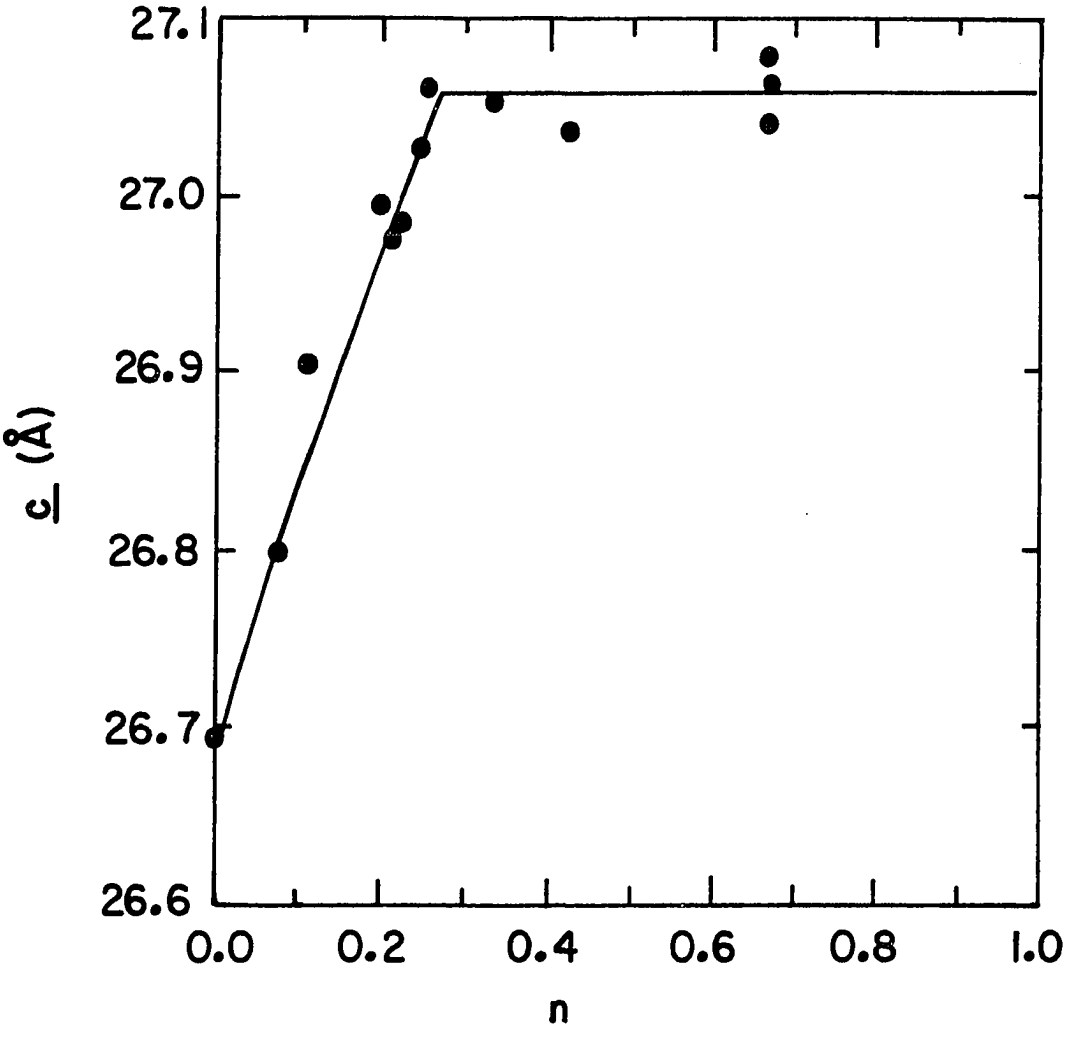

Figure 2. The c cell dimension of $ZrCl(O_y)$ vs. n from ZrCl + n ZrO_2 reactions

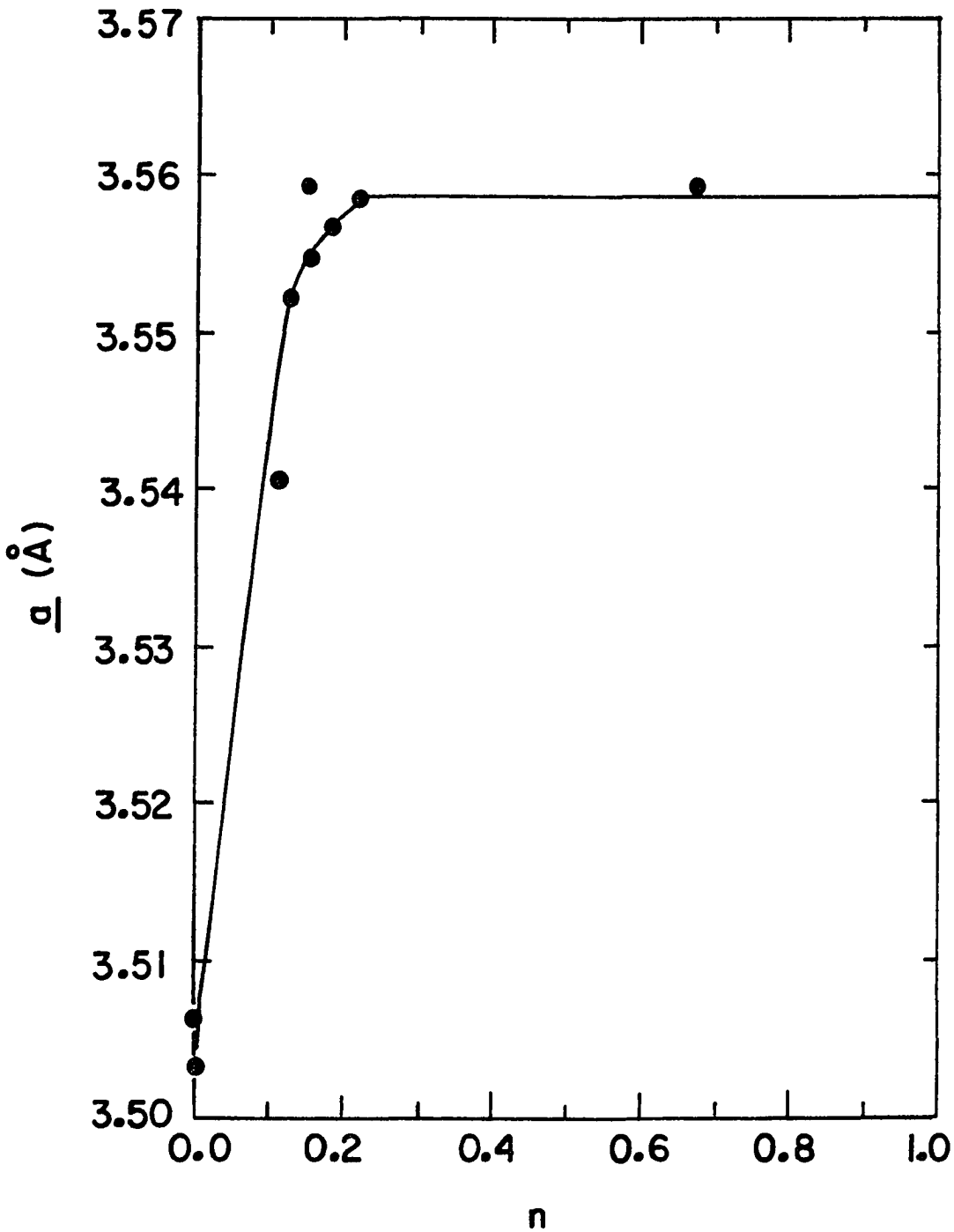

Figure 3. The a cell dimension of $ZrBr(O_y)$ vs. n from ZrBr + n ZrO_2 reactions

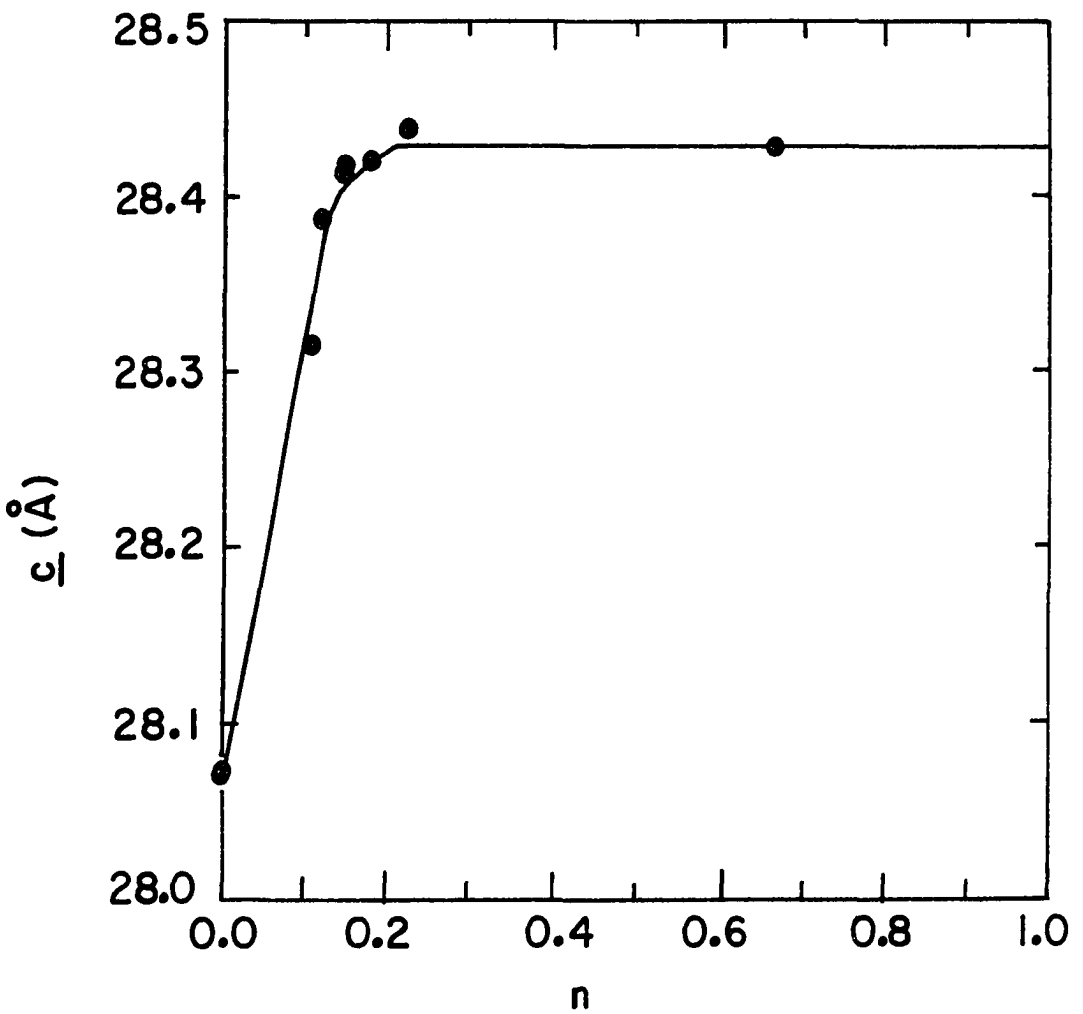

Figure 4. The c cell dimension of $ZrBr(O_y)$ vs. n from ZrBr + n ZrO_2 reactions

Table 4. Zr coproduct cell dimensions from ZrCl + n ZrO_2 reactions

n	a (Å)	c (Å)	N[a]
0[b]	3.2323(7)	5.1477(7)	9
0	3.2340(6)	5.1487(13)	10
0.08	3.2483(5)	5.2074(9)	13
0.11	3.2481(1)	5.2069(2)	9
0.20	3.2421(4)	5.2069(8)	11
0.22	3.2422(4)	5.2061(7)	13
0.23	3.2431(2)	5.2073(4)	13
0.25	3.2398(4)	5.2061(8)	10
0.26	3.2399(3)	5.2064(6)	13
0.33	3.2390(1)	5.2070(3)	8
0.43	3.2406(4)	5.2096(7)	5
0.67(I)	--[c]	--	
0.67(II)	--	--	

[a]Same as Table 2.

[b]Reference 22.

[c]Only the most intense reflections appear faintly.

Table 5. Zr coproduct cell dimensions from ZrBr + n ZrO_2 reactions

n	a (Å)	c (Å)	N[a]
0	3.2340(6)	5.1487(13)	10
0.11	3.2475(2)	5.2076(4)	9
0.13	3.2463(3)	5.2180(6)	7
0.15	3.2466(3)	5.2174(7)	11
0.18	3.2455(2)	5.2225(9)	7
0.23	3.2441(3)	5.2176(8)	7
0.67	3.239(2)[b]	5.216(8)	8

[a]Same as Table 2.

[b]Only the most intense reflections appear faintly.

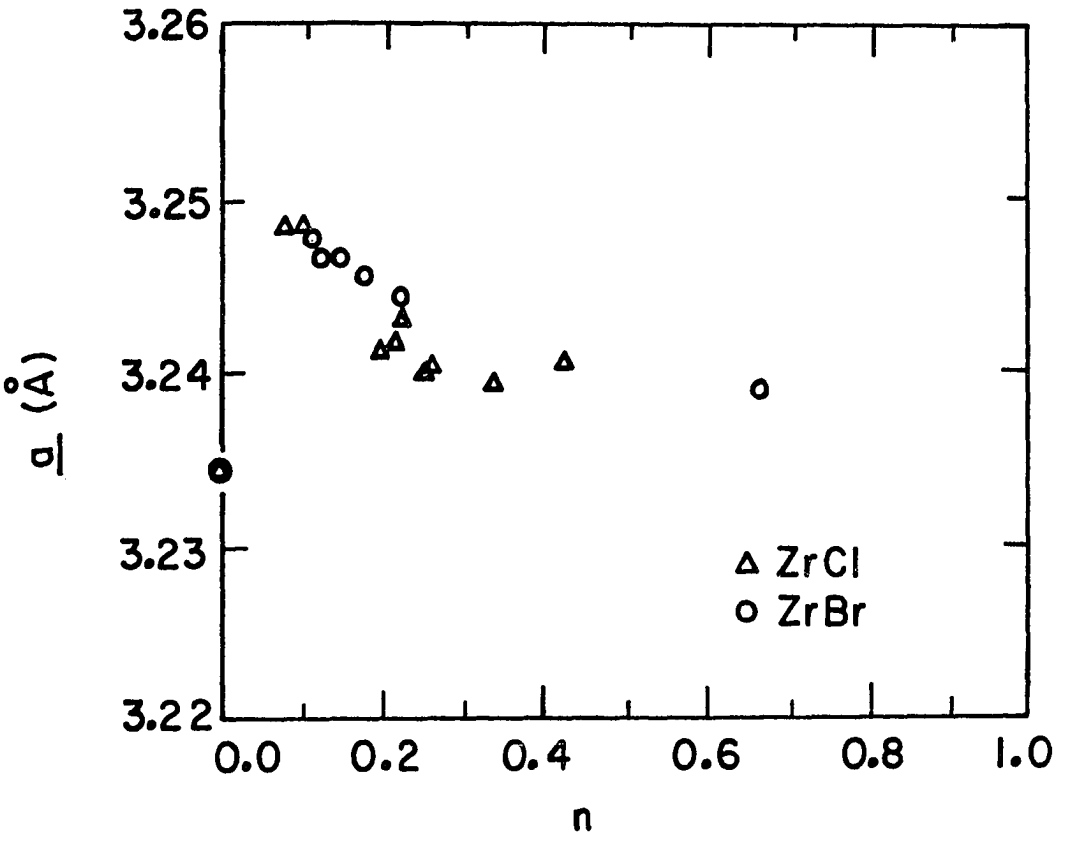

Figure 5. The a cell dimensions of the Zr coproduct vs. n from $ZrX + n\ ZrO_2$ reactions

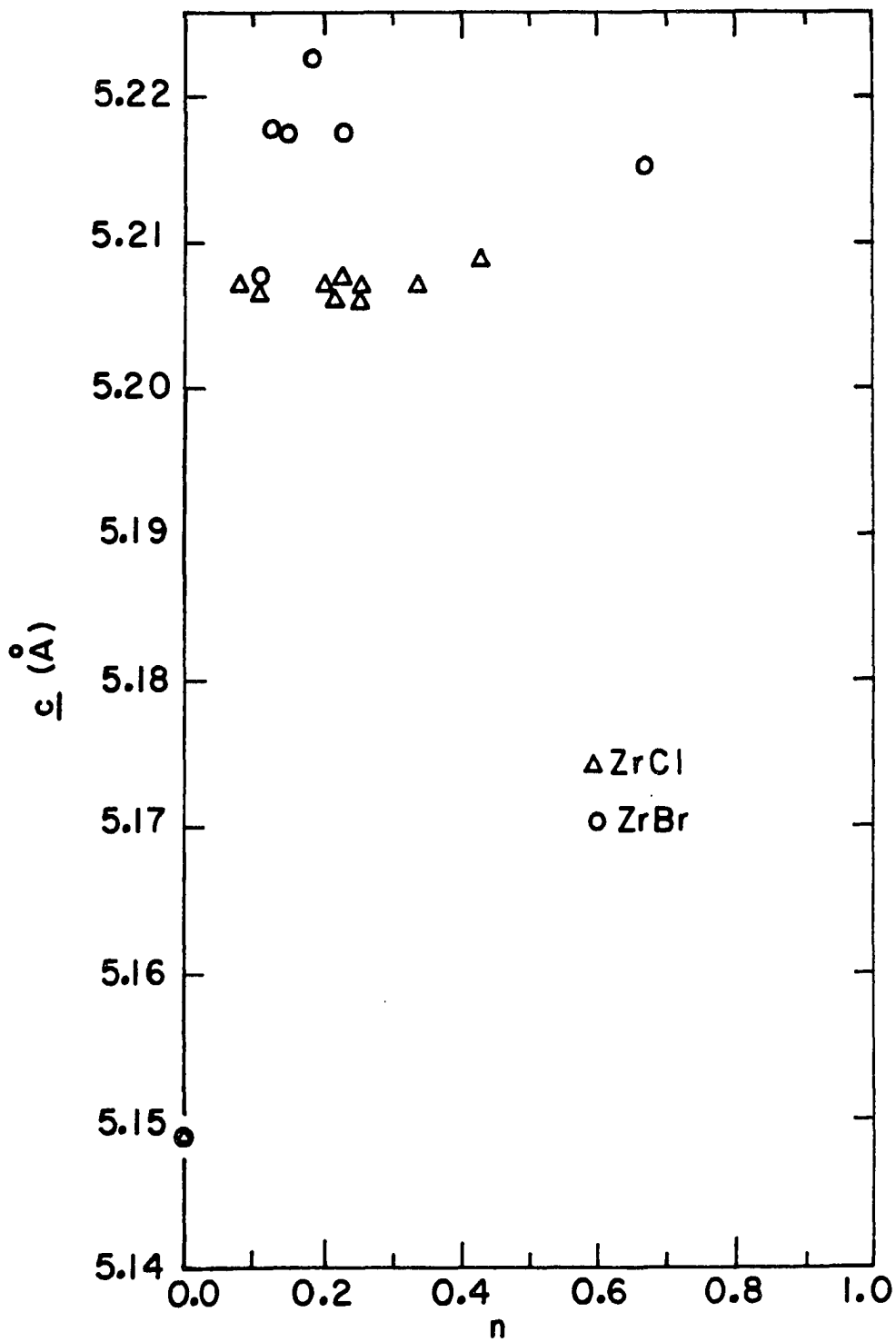

Figure 6. The c cell dimensions of the Zr coproduct vs. n from $ZrX \pm ZrO_2$ reactions

Table 6. Average lattice parameters of oxygen-saturated phases

Phase	n[a]	a	c	N(a),N(c)[b]	Δa(Å)	%a	Δc	%c
$ZrCl(O_{0.43})$	0.27±0.01	3.4956(5)	27.06(1)	6,6	+0.0723(7)[c]	2.11	+0.37(8)	1.4
$ZrBr(O_{sat})$	0.22±0.02	3.5584(4)	28.430(7)	2,2	+0.0537(6)[d]	1.53	+0.355(7)	1.26
Zr co-product								
$ZrCl(O_y)$	~0.27	3.2398(4)	5.2077(7)	3,9	-0.004(1)[e]	0.1	+0.006(1)	0.1
$ZrBr(O_y)$	~0.22	3.239(2)	5.2189(9)	1,4	-0.005(2)	0.2	+0.017(1)	0.3
$Zr(O_x)$								
This work		3.2438(3)	5.2071(9)	2,2	0	0	+0.005(1)	0.1
H+D[f]								
800°		3.2443(8)[g]	5.2030(8)	4,4	NA[h]	NA	NA	NA
1800°		3.2442(9)	5.2012(9)	3,3	NA	NA	NA	NA
ave		3.244(1)	5.202(1)		NA	NA	NA	NA

[a]Mole ZrO_2/mole ZrCl at saturation.
[b]Number of values averaged.
[c]Relative to ZrCl.
[d]Relative to ZrBr.
[e]Relative to H+D ave at oxygen saturation.
[f]Reference 22.
[g]Reference 22 gave standard deviations for only Zr metal. The assumption was made that all values were equally uncertain.
[h]Not applicable.

the c variation. The monobromide incorporated less oxygen based on the decrease in ZrO_2 for saturation ($\Delta n = 0.05$ mole) and the smaller increases of its lattice dimensions (0.58% in a, and 0.2% in c), although chloride content may have contributed to the latter apparent differences.

When $n \geq 0.67$ in either the monochloride or monobromide reactions, the Zr coproduct reflections are so faint that lattice dimensions could be determined only with high uncertainties, if at all. This is possibly due to dilution by ZrO_2. Even so, for those obtained the Zr coproducts' cell dimensions at various oxygen concentrations were anomalous relative to those reported for the Zr + n ZrO_2 by Holmberg and Dagerhamn.[22] To verify that the difference was not a systematic error, various $Zr(O_x)$ samples were prepared by reaction of Zr powder and ZrO_2 at 930° for two weeks in Ta tubing. Table 7 lists the cell dimensions and Figures 7 and 8 show the a and c dimensions vs x in $Zr(O_x)$, respectively, together with the lattice parameters of Holmberg and Dagerhamn at 800° and 1800°. These three sets of data did vary in a similar manner with increased oxygen content. The significantly larger c dimension of this work (Table 6, Figure 7) may be caused by the chloride impurity derived from the ZrO_2 used.

From the data collected, the rise and fall variation of the a lattice dimension with increased oxygen concentration observed for $Zr(O_x)$ from Zr + ZrO_2 (Figure 7) was similarly observed for the Zr coproduct from ZrX + n ZrO_2 reactions (Figure 5). Those of the latter are for all concentrations significantly ~0.005 Å smaller. The a dimension

Table 7. $Zr(O_x)$ cell dimensions from Zr (powder) + n ZrO_2

x	a	c	N[a]
0.11	3.2471(5)	5.1723(8)	12
0.25	3.2548(2)	5.1876(4)	12
0.30	3.2549(2)	5.1892(4)	13
0.32	3.2544(2)	5.1953(4)	12
0.35	3.2535(2)	5.1910(3)	12
0.40	3.2480(2)	5.2013(4)	12
0.52	3.2441(2)	5.2070(4)	13
0.64	3.2435(2)	5.2071(8)	13

[a]Number of indexed reflections used in refinement.

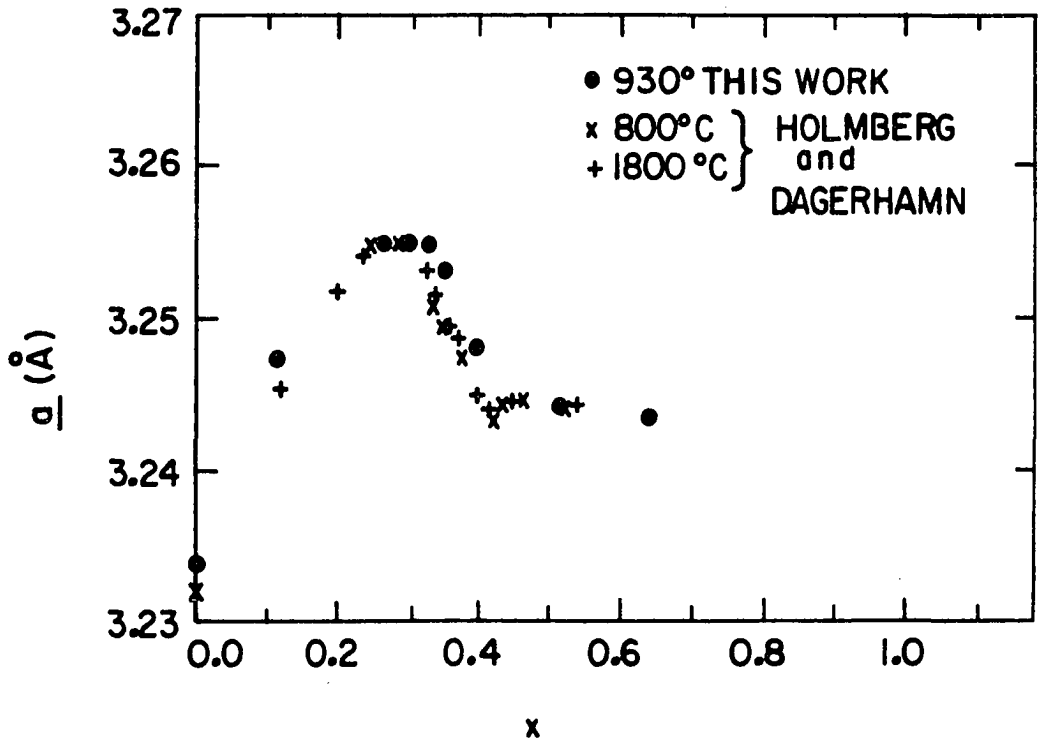

Figure 7. The a cell dimension of $Zr(O_x)$ from Zr + n ZrO_2 reactions

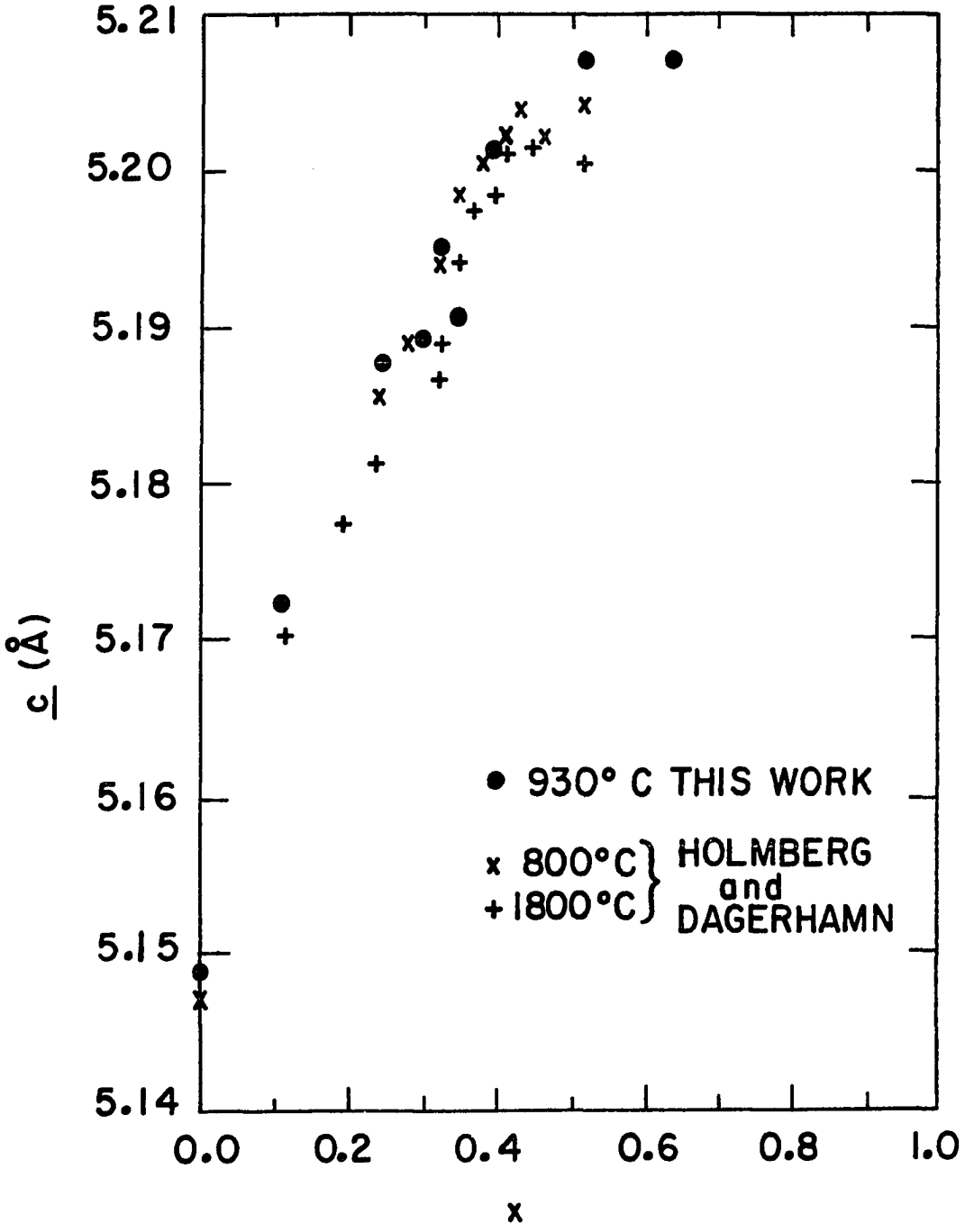

Figure 8. The c cell dimension of $Zr(O_x)$ from Zr + n ZrO_2 reactions

of monochloride Zr coproducts reasonably showed saturation at n = 0.27 ± 0.02 in agreement with the $ZrCl(O_y)$ dimensions. The a dimension of the monobromide Zr coproducts, however, because of limited data, can only be surmised to agree with the n = 0.22 mole saturation predicted by the $ZrBr(O_y)$ dimensions.

The c dimension graphs are very different. While the c dimension of $Zr(O_x)$ from Zr + n ZrO_2 reactions (Figure 8) increases steadily, although with changing slopes, with increasing oxygen concentration, the c dimensions of the Zr coproduct from ZrCl reactions are nearly constant for all oxide concentrations. The Zr coproduct c dimensions from ZrBr reactions are also nearly constant for n > 0.11 but with an expansion of 0.011(1) Å over the monochloride Zr coproduct dimensions.

The above results suggest halide solubility in the metal phase. To analyze this, 1:1 mixtures of ZrO_2 and ZrX were sandwiched between a bent Zr strip and heated at 946° for two weeks. The strips embrittled, a characteristic of oxide dissolution, but were strong enough to be cleaned with emery paper. Electron microprobe analyses found <0.1% by weight Cl and <0.05% by weight Br in the strips.

After a sample of the products of the reaction ZrCl + 0.33 ZrO_2, with Zr coproduct cell dimensions of a = 3.2390(1) and c = 5.2070(3) Å, was heated to 400° under dynamic vacuum for a few hours (Knudsen cell mass spectrometry experiment 1), however, the cell dimensions changed to 3.2426(4) and 5.2013(7) Å. This is a +0.0030(3) Å or 9σ change in a and a -0.0057 Å or 6σ change in c. No ZrCl remained in the sample. This $Zr(O_x)$ + ZrO_2 sample was later reheated to 980° under dynamic

vacuum for a few hours (Knudsen cell mass spectrometry experiment V). The lattice dimensions of the metal phase were unchanged, $\underline{a}$ = 3.2426(3) and $\underline{c}$ = 5.2013(4) Å, lending doubt to possible oxygen extraction and support to removal of chloride, as $ZrCl_4$, from the Zr coproduct in the first heating. Similar results were obtained with a sample of products from ZrCl + 0.43 ZrO_2. The Zr coproduct had lattice parameters of $\underline{a}$ = 3.2406(4) and $\underline{c}$ = 5.2096(7) Å before heating and pumping and $\underline{a}$ = 3.2433(3) and 5.2003(5) Å after. This is a 4σ increase in the $\underline{a}$ dimension and a 8σ decrease in $\underline{c}$. Again no ZrCl remained.

The two products and excess ZrO_2 where appropriate could be seen throughout the loose or sintered crystalline clumps of the reactions described in Tables 2 and 3. A top layer of larger hexagonal plates was sometimes found on the surface of a sintered clump. One such clump resulted from the reaction ZrCl + 0.26 ZrO_2. Guinier powder patterns were taken of material under the larger crystals, the middle, and the bottom of the clump to test for distribution of the three phases via relative intensities. No differences could be detected.

To test the reversibility of oxide uptake, a sample of the products of ZrCl + 0.23 ZrO_2, which would represent almost saturated phases (Tables 2 and 4) without excess ZrO_2 present, was reequilibrated with Zr powder at 930°. Indeed, the Guinier powder pattern of the new product showed the $ZrCl(O_y)$ lines shifted back very close to their positions for ZrCl, $\underline{a}$ = 3.4316(3), and $\underline{c}$ = 26.732(8) Å. The cell dimensions of the Zr coproduct correspond to a reduced oxygen concentration, $\underline{a}$ = 3.2545(2), and $\underline{c}$ = 5.1846 Å (~$Zr(O_{0.3})$). Conversely, when a

sample of low oxygen concentration from ZrCl + 0.08 ZrO_2 was reequilibrated with excess ZrO_2 at 930° for two weeks, the products contained maximum oxygen content.

The effects of temperature and heating period have been considered. Most of the reactions were subjected to a maximum of about 930°-1000° (Tables 2 and 3). All of the reactions at or after saturation were. Judging from the fit of all the points to the best curves, those corresponding to lower (890°) or higher (1016°) temperature do not appear different. Furthermore, the lattice parameters of a reaction which was cooled down at 1°/hr to 350°, the second n = 0.67 mole $ZrCl(O_y)$ reaction, gave slightly higher lattice parameters than the others at saturation, but they are not different by 3σ. To examine the effects of heating period, ZrCl + 0.23 ZrO_2 was heated with an unintentional gradient of 1016°/1002° for only six days. The resulting cell dimensions of the $ZrCl(O_y)$ phase were ~0.05 Å and ~0.03 Å less in c than predicted by the graphs, and ZrO_2 was seen in the Guinier powder pattern. Barring effects of the temperature gradient, it appears that a six day heating period is too short.

Structure results

The $ZrCl(O_{0.25})$ crystal grew from a reaction of ZrCl + 0.25 ZrO_2 + 0.25 Zr (powder) under the conditions described in Table 2. The $ZrClO_{0.29}$ crystal grew, surprisingly, from a reaction of ZrCl + 0.33 ZrS_2 in a pressed (8,000 psi) Ta tube which was heated for five weeks at 830° and cooled by shutting off the furnace. Oxygen contamination of the ZrS_2, a leak in the Ta tube container and/or glass are suspected as the source(s) of oxygen. The $ZrClO_{0.43(2)}$ was produced in the

reaction ZrCl + 0.67 ZrO_2 which was subjected to the same heating routine described for $ZrCl(O_{0.25})$.

From the Guinier powder patterns, it was observed that the ZrCl structure was being maintained but expanded in these reactions. Therefore, the first step of refinement of the structure inserted the Zr and Cl at the positions of ZrCl.[7] Full matrix least squares refinement using isotropic thermal parameters gave an unweighted residual of $R = \sum||F_o| - |F_c||/\sum|F_o| = 0.102, 0.072, 0.047$ and $R_w = [\sum w(|F_o| - |F_c|)^2/\sum w|F_o|^2]^{1/2} = 0.143, 0.109, 0.059$ for y = 0.25, 0.29, 0.43, respectively. Conversion to anisotropic thermal parameters yielded R = 0.090, 0.072, 0.046 and R_w = 0.137, 0.109, 0.057, respectively.

At this point, the oxygen position appeared in the tetrahedral-like interstice between the Zr layers on each structure's electron density and electron density difference maps. Refinement of this position in the $ZrCl(O_{0.25})$ case may have been somewhat influenced by a small occupancy neighboring it which appeared on the electron density map but did not appear on the difference map. The peak was verified as being insignificant by assignment of an oxygen there and variation of its position and multiplier which resulted in 0.00(6) for the latter. The other two structures did not show any other residuals.

Attempts to allow the oxygen to have anisotropic thermal parameters in $ZrCl(O_{0.25})$ and $ZrCl(O_{0.29})$ resulted in very large unreasonable Bs. When isotropic thermal parameters were allowed to vary at several selected occupancies (0.1 - 1.0), a negative value always resulted.

For these reasons, oxygen was assigned the isotropic thermal parameters of Cl, 0.7 $Å^2$. Any variation of both the oxygen occupation factor and the isotropic temperature factor could be done with reasonable results only with $ZrCl(O_{0.43})$. Here the resulting B(O) = 1.5(3) $Å^2$ is close to that of Cl (1.74(5) $Å^2$) and Zr (1.64(4) $Å^2$). The thermal parameters of this structure are larger than the others, suggesting some distortions and possibly a superstructure, especially since saturation has been reached. To the x-ray techniques of oscillation, zero- and first-level Weissenberg photos, no superstructure spots could be detected. Final refinement yielded y = 0.25(5), 0.29(4), and 0.43(2) with R = 0.081, 0.059, 0.046 and R_w = 0.120, 0.084, and 0.056, respectively.

Table 8 compares the lattice constants, atomic positions and thermal parameters, Table 9 compares the interatomic distances, Table 10 compares the interatomic angles common to ZrCl, and Table 11 compares the interatomic distances and angles of the Zr_4O tetrahedra. Figures 9 and 10 show the ORTEP drawings of three slabs in a 110 projection and an isolated Zr_4O tetrahedron, respectively, for $ZrCl(O_{0.43})$. The structure factor lists for y = 0.25(5), 0.29(4), and 0.43(2) appear in APPENDICES A, B, and C, respectively.

The $ZrBr(O_y)$ crystal was produced in the reaction ZrBr + 0.15 ZrO_2 under the conditions described in Table 3. Its lattice dimensions (Table 12) determined from LATT are insignificantly different from but are 0.0010(6) Å larger in a and 0.012(9) Å less in c than in saturated $ZrBr(O_y)$ and also 0.0053(5) Å larger in a and 0.006(6) Å larger in c than the lattice dimensions determined from Guinier powder pattern data

Table 8. Lattice constants (Å), atomic positions, and thermal parameters of ZrCl and $ZrClO_y$ (Trigonal cell, $R\bar{3}m$, Z=6)[a]

	ZrCl a=3.4233(5)[b] c=26.693(3)		$ZrClO_{0.25}$ a=3.4912(3) c=27.002(9)		
	Zr	Cl	Zr	Cl	O
Z	0.1221(1)	0.3901(3)[c]	0.1211(1)	0.3895(4)	0.207(4)
B_{11}[e]	0.4(2)	0.6(3)	0.3(2)	0.4(3)	0.7[d]
B_{33}	0.51(4)	0.52(6)	1.0(2)	1.1(4)	

[a] $x=y=0$, $B_{11}=B_{22}=1/2\ B_{12}$, $B_{13}=B_{23}=0$.

[b] Reference 8.

[c] Reference 7.

[d] Assigned.

[e] B in $Å^2$.

$ZrCl(O_{0.29})$ $\underline{a}$=3.4926(3) $\underline{c}$=27.025(8)			$ZrCl(O_{0.43})$ $\underline{a}$=3.4984(2) $\underline{c}$=27.065(4)		
Zr	Cl	O	Zr	Cl	O
0.12111(9)	0.3897(3)	0.202(2)	0.12084(4)	0.3895(1)	0.2001(6)
0.56(7)	0.7(2)	0.7[d]	1.58(4)	1.63(6)	1.5(3)
0.4(1)	0.7(2)		1.72(5)	1.85(9)	

Table 9. Interatomic distances for $ZrCl(O_y)$

					% increase from ZrCl		
y =	0	0.25	0.29	0.43	0.25	0.29	0.43
Intralayer[a]	3.4233(5)[b]	3.4912(3)	3.4926(3)	3.4984(2)	1.98	2.02	2.19
Interlayer							
Zr-Zr	3.087(5)[c]	3.181(4)	3.183(4)	3.199(2)	3.0	3.1	3.6
Cl-Cl	3.61(1)	3.64(2)	3.65(4)	3.648(5)	0.8	1	1
O-O	--	2.97(16)	2.78(10)	2.71(3)	--	--	--
Zr-Cl	2.629(6)	2.671(7)	2.669(5)	2.673(2)	1.6	1.5	1.7
Zr_{apex-O}	--	2.32(11)	2.19(7)	2.15(2)	--	--	--
Zr_{base-O}	--	2.021(8)	2.035(10)	2.047(3)	--	--	--

[a]Intralayer Zr-Zr = Cl-Cl = O-O.

[b]Reference 8.

[c]Reference 7.

Table 10. Interatomic angles (deg) common to ZrCl and $ZrCl(O_y)$[a]

Atom 1	Atom 2	Atom 3	y = 0[b]	0.25	0.29	0.43
Zr(1)	Zr(4)	Zr(103)	67.4(1)	66.6(1)	66.6(1)	66.30(4)
Zr(204)	Zr(4)	Zr(2)	60.00	60.00	60.00	60.00
Zr(4)	Zr(2)	Zr(104)	120.00	120.00	120.00	120.00
Zr(4)	Zr(2)	Zr(103)	56.32(6)	56.72(5)	56.72(5)	56.85(2)
Cl(2)	Zr(2)	Zr(103)	105.4(1)	105.6(1)	105.5(1)	105.63(4)
Cl(2)	Zr(2)	Zr(4)	49.4(1)	49.2(1)	49.14(9)	49.13(4)
Cl(2)	Zr(2)	Cl(104)	81.2(2)	81.6(3)	81.7(2)	81.73(8)
Zr(2)	Cl(2)	Zr(104)	81.2(2)	81.6(3)	81.7(2)	81.73(8)

[a]Atom numbers correspond to those in Figures 1 and 2 of Reference 7.

[b]Reference 7.

Table 11. Interatomic distances and angles of a Zr_4O in $ZrCl(O_y)$

y =	0.25	0.29	0.43
Distances (Å)			
Zr_B-Zr_B[a]	3.4912(3)	3.4926(3)	3.4984(2)
Zr_B-Zr_A	3.181(4)	3.183(4)	3.199(2)
Zr_A-O	2.32(11)	2.19(7)	2.15(2)
Zr_B-O	2.021(8)	2.035(10)	2.047(3)
Angles (deg)			
Zr_B-Zr_B-Zr_B	60.00	60.00	60.00
Zr_A-Zr_B-Zr_B	56.72(5)	56.72(5)	56.85(2)
Zr_B-Zr_A-Zr_B	66.57(10)	66.55(10)	66.30(4)
Zr_B-Zr_A-O	39.32(6)	39.31(6)	39.16(3)
Zr_B-Zr_B-O	30.2(4)	30.9(5)	31.3(1)
Zr_A-Zr_B-O	47(3)	43(2)	41.5(5)
Zr_B-O-Zr_B	119.5(7)	118.3(9)	117.4(3)
Zr_A-O-Zr_B	94(3)	98(2)	99.4(5)

[a] Zr_A = apex Zr, Zr_B = base Zr of tetrahedron. See Figure 10.

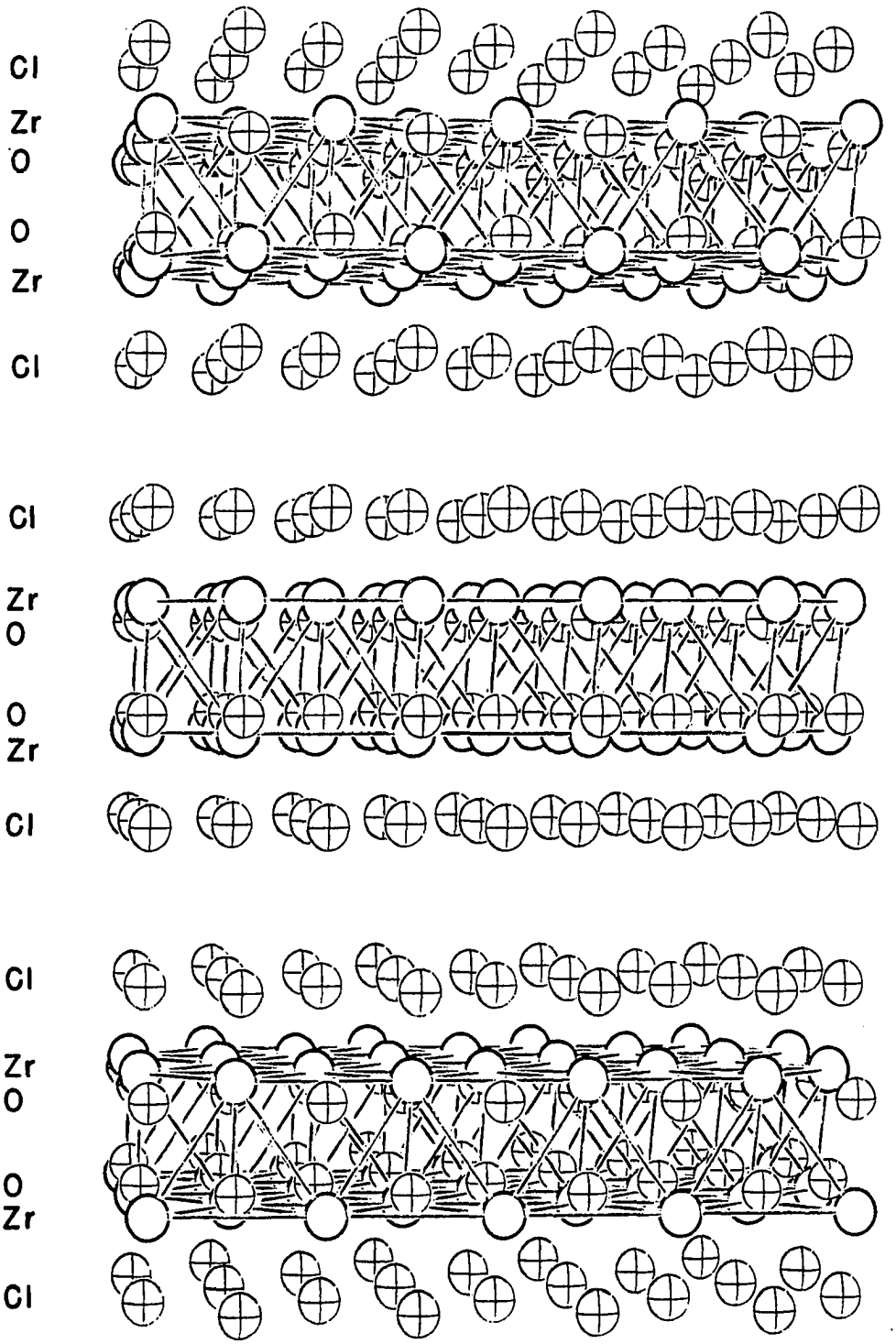

Figure 9. Three slabs in the 110 projection of $ZrCl(O_{0.43})$. The a axis is the intralayer interatomic distance. The c axis is vertical

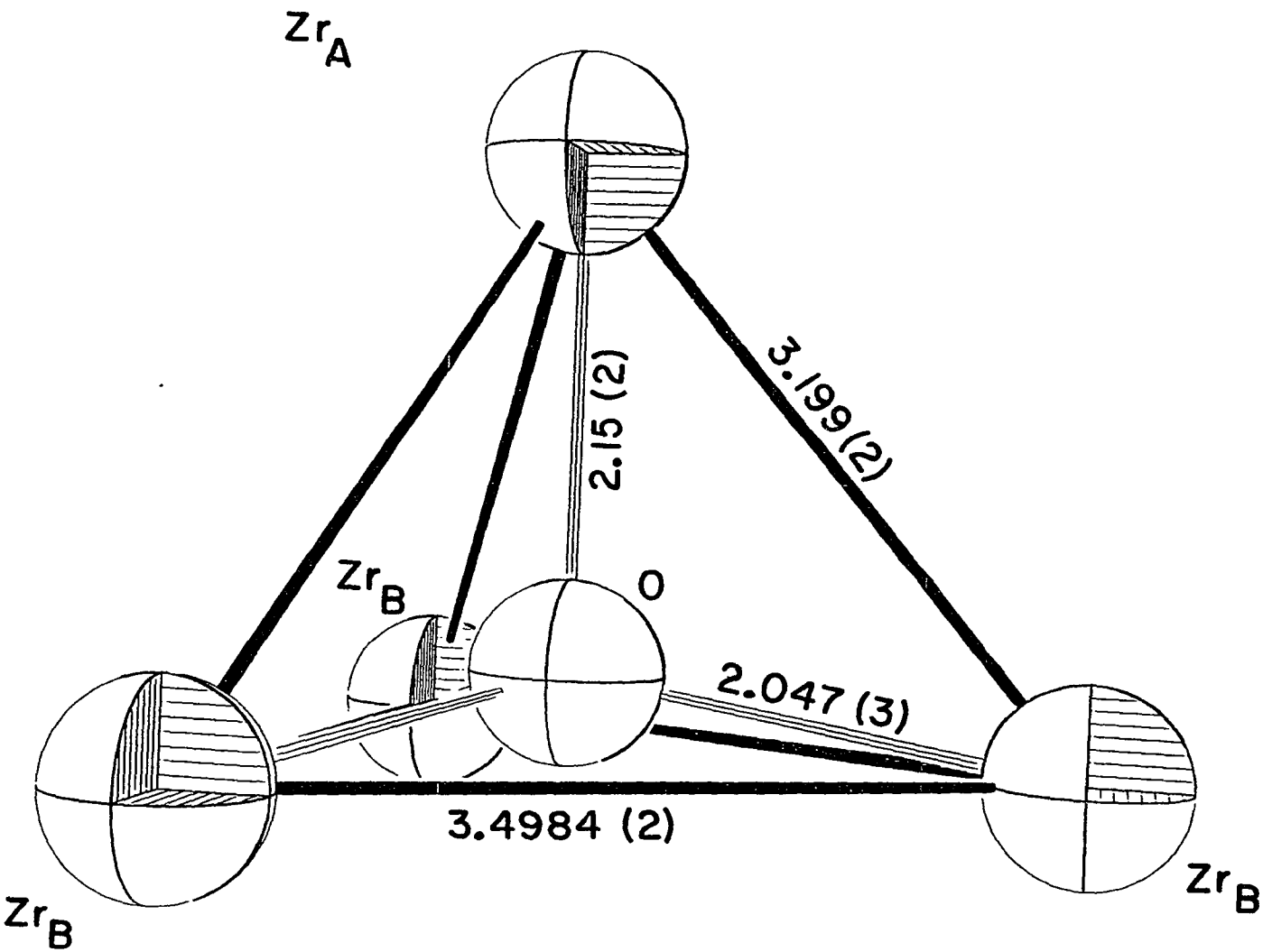

Figure 10. An isolated Zr_4O tetrahedron in $ZrCl(O_{0.43})$

Table 12. Atomic positions and thermal parameters for ZrBr and $ZrBr(O_{0.29(6)})$ (trigonal, R3m, Z=6)[a]

	ZrBr[b] a=3.5031(3) c=28.071(3)		$ZrBr(O_{0.29(6)})$ a=3.5594(4) c=28.418(5)		
	Zr	Br	Zr	Br	O
z	0.2092(4)	0.3917(5)	0.2092(2)	0.3903(2)	{0.137[c] 0.108(3)[d]
B_{11}[c,e]	--	--	1.3(2)	1.3(2)	
B_{33}	--	--	0.7(3)	0.7(3)	
$B_{isothermal}$	0.5	1.9(4)			0.7

[a] $x=y=0$, $\beta_{11}=\beta_{22}=1/2\ \beta_{12}$, $\beta_{13}=\beta_{23}=0$.

[b] Reference 8.

[c] Position observed on election density map.

[d] Refined position.

[e] B in $Å^2$.

for this reaction.

As with the $ZrCl(O_y)$ crystals, the positions and isotropic thermal parameters of ZrBr[8] were initially selected because the powder patterns showed the ZrBr structure was being maintained and expanded. Conversion to anisotropic thermal parameters yielded R = 0.094 and R_w = 0.183. An occupancy in the tetrahedral-like site between the Zr layers (0, 0, 0.137) was observed on the electron density map. Assignment of it as oxygen with B = 0.7 $Å^2$ followed by variation of the occupancy factor and position yielded $ZrBr(O_{0.29(6)})$ but the position refined just into the region between the Zr and Br layers at (0, 0, 0.108(3)) with R = 0.094, and R_w = 0.170. There is no electron density at this site on the electron density or difference map. No other possible electron densities are real. Several other attempts to refine this structure were unsuccessful. Table 12 compares the lattice constants, atomic positions, and thermal parameters, while Table 13 compares the interatomic distances of Zr and Br only in ZrBr and $ZrBr(O_{0.29})$. The structure factor list for $ZrBr(O_{0.29(6)})$ appears in APPENDIX D.

Balanced equations

In the worse case, with the chloride impurity in the ZrO_2 (Cl:Zr = 0.07 by mole by x-ray fluorescence), this reactant can be simply thought of as $ZrO_{1.97}Cl_{0.07}$. Since saturation for the ZrCl reactions occurred with n = 0.27 ± 0.01 to give $ZrCl(O_{0.43(2)})$ and, neglecting the minute Cl^- content, $Zr(O_x)$, an equation can be written and solved for the oxygen content in $Zr(O_x)$:

$$ZrCl + 0.27\ ZrO_{1.97}Cl_{0.07} \rightarrow 1.02\ ZrCl(O_{0.43}) + 0.25\ ZrO_{0.37}\ .$$

Table 13. Interatomic distances of Zr and Br only in ZrBr and $ZrBr(O_{0.29})$

	ZrBr[a]	$ZrBr(O_{0.29})$	% increase
Intralayer	3.5031(3)	3.5594(4)	1.16
Interlayer			
Zr-Zr	3.130(12)	3.17[b]	1
Br-Br	3.85(2)	3.84	0
Zr-Br	2.74(1)	2.80	2

[a]Reference 8.

[b]ALLS output.

Within the uncertainty limits of the empirically determined values for n, y, and the analyzed chloride impurity, x varies from 0.30 to 0.43. Thus, the oxygen content is reasonably close to that reported for saturation, $Zr(O_{0.42})$.[22] If no chloride impurity and $Zr(O_{0.42})$ are assumed, and the above reaction is solved for n, again n = 0.27. Thus, the following can be assumed to describe the reaction at saturation between ZrCl and ZrO_2:

$$ZrCl + 0.27\ ZrO_2 \xrightarrow[2\ wk]{850\text{-}1000^\circ} ZrCl(O_{0.43}) + 0.27\ Zr(O_{0.42}) .$$

Similarly, assuming $Zr(O_{0.42})$ and including the chloride impurity, an equation can be written for the monobromide oxide at saturation where n = 0.22 ± 0.02 and solved for the stoichiometry of $ZrBr_{1-x}Cl_x(O_y)$:

$$ZrBr + 0.22\ ZrO_{1.9}Cl_{0.07} \rightarrow 0.99\ ZrBr_{0.98}Cl_{0.02}(O_{0.34}) + 0.23\ Zr(O_{0.42}) .$$

Electron microprobe analysis of this phase found Br:Zr = 0.97 and Cl:Zr = 0.04. The above oxygen concentration of this phase does not deviate within the uncertainty limits of the empirically determined values of n at saturation and the chloride impurity. Assuming no chloride impurity, an almost identical oxygen content in $ZrBr(O_y)$ is obtained, y = 0.35. Thus, the following can be assumed to describe the reaction at saturation:

$$ZrBr + 0.22\ ZrO_2 \xrightarrow[2wk]{1000^\circ} ZrBr(O_{0.35}) + 0.22\ Zr(O_{0.42}) .$$

Notice that ZrBr incorporates 0.08 mole less oxide than ZrCl. This is consistent with the smaller n and lattice dimension increases at saturation. The reason for this is not obvious, but the different stacking orders of ZrCl and ZrBr and the greater electronegativity of Cl^- over Br^- could contribute.

The chloride impurity incorporation into the bromide oxide could explain why Daake found the lattice dimensions of saturated $ZrBr(O_y)$ to be $\underline{a}$ = 3.5646(2) and $\underline{c}$ = 28.479(5) Å which are significantly larger than found in this work (Table 6) by 0.0062(4) Å in $\underline{a}$ and 0.049(9) Å in $\underline{c}$. Ziebarth[44] recently independently confirmed Daake's lattice dimensions for $ZrBr(O_y)$ at saturation. All three researchers are in agreement on the lattice dimensions at saturation for $ZrCl(O_y)$. Again, as with the Zr coproduct, a very small chloride incorporation has a noticeable effect on the lattice dimensions.

Transport reactions

$ZrX(O_y)$ transports to the cool end of a ~950°/~500° temperature gradient leaving the Zr coproduct and any ZrO_2 behind. Table 14 contains the data on these reactions. The $ZrX(O_y)$ plates produced are seldom single as they grow on top of each other face to face and are irregularly shaped but with some trigonal morphology. Crystals of $ZrX(O_y)$ from n = 0.23 were relatively large (2 x 2 x 0.005 mm) and represented 80% of the contents of the reaction. Usually a small amount of ZrX_4 deposited at the extreme cool end, possibly from the faster cool down of this end when the furnace was shut off. Caution must be taken during the reaction to keep the cool end above the ZrX_4 deposition temperature.

The ZrBr system had the additional problem of $ZrBr_3$ instead of $ZrBr(O_y)$ deposition at the cool end if the temperature was favorable (~350-450°[10]). As a crude indicator of the temperature at the cool end, thermocouples were placed outside the fused silica jacket. These measurements were estimated to be 150-200° below the temperature at the cool

Table 14. Transport reactions, heating histories, and products[a]

Sample	$n^{b}_{initial}$	$T_1°/T_2°$[c]	ZrCl(O_y) (cool end)				Zr phase (hot end)			
			a(Å)	c(Å)	N^{d}	$\sim n^{e}_{final}$	a(Å)	c(Å)	N^{d}	Id.[f]
Started with ZrCl + n ZrO_2:										
ZrCl	0	936/216	3.4866(3)	26.960(7)	6	0.20	3.2439(1)	5.1681(3)	12	$Zr(O_{0.10})$
	0.23	945/217	3.4608(7)	26.82(2)	8	0.10	3.2446(3)	5.2001(6)	12	$Zr(O_{0.40})$
	0.50	936/216	3.4991(4)	27.04(1)	6	0.27	3.2387(2)	5.2087(6)	13	n=0.27
ZrBr	0.50	936/216	3.5590(2)	28.411(5)	20	0.22	3.2414(3)	5.2068(5)	12	$Zr(O_{0.41})$
Started with products of previous isothermal reaction:										
ZrCl	0.08	930/360	3.4963(2)	27.07(1)	7	0.27	3.2510(1)	5.2124(3)	12	$>Zr(O_{0.41})$(?)
	0.20	930/360	3.4975(6)	27.05(3)	6	0.27	3.2417(2)	5.2058(4)	12	n=0.21
ZrBr	0.18	930/360	--[g]	--	--	--	3.2448(2)	5.2069(3)	12	$Zr(O_{0.40})$

[a]Reactants start at hot end.
[b]Initial n = mole ZrO_2/mole ZrCl.
[c]Two weeks.
[d]Number of indexed reflections used in refinement.
[e]n for transported product from lattice parameters. See Figures 1-4.
[f]Identification of Zr phase composition. See Figures 5-8. "n=" means lattice dimensions correspond to Zr coproduct from ZrCl + n ZrO_2 reaction. $Zr(O_x)$ means lattice dimensions correspond Zr phase from Zr + ZrO_2 reaction.
[g]Lattice parameters not obtained.

end of the Ta tube. This combined with the rapid drop in temperature of the jacket outside the tube furnace made regulation of the cool end temperature difficult.

Unoxygenated ZrCl does not transport. ZrCl alone yielded 5% of the contents as unsaturated $ZrCl(O_y)$ crystal (Table 14) 1.5-3.5 cm from the cool end of the tube. The oxygen must be from impurity glass or residual oxygen in the Ta, etc. The bulk of the contents was in a clump at the hot end with large ($4 \times 4 \times 0.005$ mm), well-formed crystals on top. The Guinier powder pattern of the clump and crystals showed only an unshifted ZrCl pattern plus a shifted Zr pattern (Table 14) in the ratio of 2:1. Some $ZrCl_4$ deposited at the cool end also. The lattice constants of the Zr coproduct are 0.099(6) Å larger in the a dimension and 0.019(1) larger in the c dimension than in the metal. This expansion approximately corresponds to $Zr(O_{0.08})$ (Figures 7 and 8). It is not presently understood why this oxygenated Zr and ZrCl would coexist at these temperatures. Perhaps with a longer reaction time the rest of the oxygen would have been deposited as $ZrCl(O_y)$ at the cool end.

Table 14 shows that most often the $ZrX(O_y)$ deposited at the cool end had lattice dimensions very close to saturation after transport. When the products of previous reactions which were less than saturated were used, the lattice dimensions of the transported $ZrCl(O_y)$ crystals indicated approximate saturation. However, for n = 0.23 and 0, the $ZrCl(O_y)$ did not have the fully expanded lattice dimensions indicative of saturation. The 0.23 reaction had smaller lattice dimensions, indicating less oxygen, than the separately conducted 0.23 experiment. A mistake could

have been made in the amount of ZrO_2 added in one of these experiments. The metal phase gave a variety of results and the reader is referred to the comments on the table. Interestingly, sometimes the lattice dimensions seem to be of $Zr(O_x)$ as when only zirconium and oxygen are in the system. Apparently the chloride was removed via $ZrCl_4$ as reported earlier.

Knudsen cell mass spectrometry study

This study was undertaken to attempt to identify oxygen-containing vapor species responsible for the transport of $ZrCl(O_y)$. Table 15 lists the samples studied, the orifice sizes and the top cap attachments used, the highest temperatures reached, the species observed in the mass spectrum (MS), and the compounds identified in the Guinier powder pattern taken after the experiment.

The 13 mil orifice of Experiment I allowed a $ZrCl_4$ pressure in the instrument so high (5×10^{-5} torr) when the temperature was raised rapidly that the instrument had to be shut off. Later the temperature was increased more slowly to make sure the $ZrCl_4$ gas was not generated suddenly at a specific temperature which would indicate a solid phase change. This time the MS peaks were found to grow with temperature which eliminates this possibility. After the experiment, the Guinier powder pattern showed only the $Zr(O_x)$ phase (General reactions section) and ZrO_2 with no $ZrCl(O_y)$. Apparently the $ZrCl(O_y)$ had all disproportionated.

Experiment V used a similar sample but with a 4 mil orifice and a mostly welded cap which prevented the pressure from exceeding 10^{-5} - 10^{-4} torr. The same peaks as seen in Experiment I were observed. A maximum temperature of 935° was reached but by then the intensities

Table 15. Conditions and results of Knudsen cell mass spectrometry experiments

Sample	Orifice size and cap attachment	Highest T	Species observed in MS	Guinier powder pattern after experiment
I. Products of $ZrCl + 0.33\ ZrO_2$: $ZrCl(O_{max}) + Zr(O_x) + ZrO_2$	13 mil not welded	~400°C	$ZrCl_4^+$, $ZrCl_3^+$ $ZrCl_2^+$, $ZrCl^+$ Cl^+, HCl^+, ClO^+	$Zr(O_x) + ZrO_2$
II. Beginning with starting materials: $ZrCl + 0.33\ ZrO_2$	4 mil welded	675°C	Same as Exp. I but didn't check for ClO^+.	$ZrCl + ZrO_2 + Zr$
III. $ZrCl_4$ alone	4 mil not welded	172°C	Same as Exp. I very small ClO^+	Not taken
IV. Remains after Exp. I: $Zr(O_x) + ZrO_2$	13 mil not welded	980°C	No peaks	$Zr(O_x) + ZrO_2$
V. Products of $ZrCl + 0.33\ ZrO_2$ $ZrCl(O_{max}) + Zr(O_x) + ZrO_2$	5 mil welded	935°C	Same as Exp. I	$Zr(O_x) + ZrO_2$

were very weak.

Experiments II, III, and IV were performed to identify the peaks observed. $ZrCl_4$ showed the same peaks in the same relative intensities as Experiments I and V above but very small peaks at ClO^+ region. The relative heights of the major peaks were as observed by Khodeev and Tsirel'nikov,[45] 85% $ZrCl_4^+$, 100% $ZrCl_3^+$, 26% $ZrCl_2^+$, 19% $ZrCl^+$, and 11% Zr^+, except the present work did not detect Zr^+. Similarly, Experiment II which began with the reactants ZrCl + 0.33 ZrO_2 showed the same peaks as $ZrCl_4$. Its Guinier powder pattern showed only ZrCl, ZrO_2, and Zr, indicating that mainly only the disproportionation of ZrCl must have occurred. Experiment IV used the $Zr(O_x)$ and ZrO_2 left after Experiment I to see if any zirconium oxide vapor was detectable; none was, even at 980°.

Thermodynamic calculations were prevented because of the unshutterability of the peaks observed after a time and the inability to achieve equilibrium. The peaks fell in intensity with time even between adjacent scans. This also prevented identification of parent and daughter peaks.

Analogous reaction attempts

ZrS_2, ZrS (WC-type), ZrS (NaCl-type), ZrN, ZrF_4, and ZrC were tried with ZrCl to form products analogous to $ZrX(O_y)$ or other interesting ternary phases. The solubility of the anions in the Zr metal were, when possible, checked via the phase diagram. Nitrogen has an appreciable solubility limit of $Zr(N_{0.37})$ and $Zr(N_{0.004})$ for α- and β-Zr, respectively,

at 1000°.[46] Carbon and sulfur have no measured solubility. The fluoride phase diagram was unavailable.

ZrS_2 was tried in various amounts with ZrCl or $ZrCl_4$ + 3 Zr at temperatures from 500°-1000°. Severe reaction with the Ta tube container resulted above 850°. Those below resulted in other zirconium sulfides: ZrS (WC-type), ZrS (NaCl-type), ZrS_3, and Zr_3S_4. Reaction of ZrS_2 with Zr metal from ZrCl disproportionation is probably the cause of the reduced sulfides because $ZrCl_4$, but no ZrCl, was found in the powder patterns. However, ZrCl was found to scavenge oxygen in two reactions (Structure results). A few unidentified reflections were seen in the powder patterns which could be due to a new ternary phase but no new phase could be visually detected.

$ZrS_{0.867}$ (WC-type ZrS) and $ZrS_{1.29}$ (NaCl-type) were used as reduced sulfides. Nothing encouraging resulted. Equal molar amounts of $ZrS_{1.29}$ and ZrCl at 592°/597° for two weeks in a pressed tube (8,000 psi) yielded products identified by Guinier powder patterns and/or visual examinations as ZrS (WC-type), ZrS (NaCl-type), $ZrCl_4$, and ZrCl without apparent changes. Again, the ZrCl probably caused the reduction of $ZrS_{1.29}$. Under similar conditions $ZrS_{0.867}$ showed no reaction. At 971°/946°, the Guinier powder pattern showed ZrS (WC-type), shifted Zr, $ZrCl_4$, and a faint ZrCl pattern.

ZrN was tried with various amounts of ZrCl at 910-930°. Shifted ZrCl and shifted Zr powder patterns resulted. A transport reaction, ZrCl + 0.99 ZrN, with a 930°/360° (outside fused silica jacket) temperature gradient was performed to isolate the possible $ZrCl(N_y)$ phase.

When opening the Ta tube in the ESCA drybox, black plate crystals and a little $ZrCl_4$ were found deposited at the cool end while a fine dark powder remained at the hot end. XPS examination of the plates detected zirconium, chlorine, and oxygen but no nitrogen (Photoelectron spectroscopy section). XPS examination of the powder detected zirconium, chlorine, nitrogen and a small amount of oxygen (probably from the tape or probe). XPS examination of the ZrN starting material found a lot of oxygen which disappeared only with multiple etchings. Thus, as in the ZrS_2 reaction, ZrCl was found to scavenge oxygen. Guinier powder patterns of the hot end material found ZrN and an expanded Zr metal phase with lattice dimensions of $\underline{a}$ = 3.2584(4) and $\underline{c}$ = 5.2255(11) Å. These dimensions are ~0.02 Å larger than in the most expanded Zr co-product from ZrX + n ZrO_2 but are close to the values reported for nitrogen saturated α-Zr, $\underline{a}$ = 3.262(?) and $\underline{c}$ = 5.220(?) Å determined via Debye-Scherrer data.[47] No $ZrCl(O_y)$ or ZrCl was detected at the hot end. The Guinier powder pattern of the cold end material found $ZrCl_4$ and expanded ZrCl patterns with lattice constants of $\underline{a}$ = 3.4885(1) Å and $\underline{c}$ = 27.040(8) Å. These correspond to lattice dimensions observed for n ≃ 0.25 mole (Table 3, Figures 1 and 2), which is only 0.02 mole away from saturation (Table 6).

ZrF_4 was tried in two reactions, ZrCl + 0.02 ZrF_4 and ZrCl + 0.10 ZrF_4, heated at 1003°/989° for three weeks. Sintered black clumps were found on opening the tube with the latter reaction having ZrF_4 deposited throughout the tube and the former having only a trace. The Guinier powder pattern of the former showed a slightly shifted ZrCl pattern, a

shifted Zr pattern, and a number of unidentified reflections. The latter reaction gave the same results but without shifting of the ZrCl pattern. As this had far more ZrF_4 available, the shifting of the ZrCl pattern in the first reaction is probably due to oxygen impurity. The unidentified lines may be something interesting but were not pursued. The lattice constants of the expanded Zr phase of the first and second reaction are $\underline{a}$ = 3.2533(7) and $\underline{c}$ = 5.1946(7) Å, and $\underline{a}$ = 3.2517(4) Å and $\underline{c}$ = 5.1809(7) Å, respectively. The $\underline{a}$ parameters are significantly greater while the $\underline{c}$ parameters are significantly lower than those typical of the ZrO_x system, indicating absorption of fluorine and/or oxygen.

ZrC was tried in the reaction ZrCl + 0.15 ZrC at 921°/958° for two weeks. The Guinier powder pattern showed unchanged ZrCl, ZrC, and again a shifted Zr pattern with lattice constants $\underline{a}$ = 3.250(7), $\underline{c}$ = 5.186(1) Å, which is probably a result of oxygen impurity.

None of the above attempts clearly produced a shifted ZrCl powder pattern indicative of a phase analogous to $ZrCl(O_y)$, which could not be attributed to $ZrCl(O_y)$. In fact, ZrCl tends to be selective to oxygen as discovered in the ZrS_2 and ZrN reactions. The unidentified lines in the powder patterns in the ZrS_2 reactions below 850° and ZrF_4 reactions could represent new ternary phases. No new phases could be visually found. The expanded Zr phases found in the ZrN and ZrC reactions are surmised to arise from either nitrogen in the ZrN reactions and/or oxygen impurity.

Photoelectron spectroscopy of $ZrCl(O_{\sim 0.43})$ and ZrCl

The $ZrClO_{\sim 0.43}$ used was found at the cool end of the transport reaction containing contaminated ZrN as described above. The ZrCl was newly prepared. Figure 11 shows the XPS for the $Zr(3d)_{3/2}$ and $Zr(3d)_{5/2}$ from $ZrClO_{\sim 0.43}$. The small shoulder at 185.5 eV could be from $ZrCl_4$.[48,49] The two $ZrCl_4$ peaks could be a contribution to the $Zr(3d)_{3/2}$ peak with the result that the relative intensities of the Zr(3d) peaks reversed from those of other zirconium chlorides.

Figure 12 shows the XPS for the $Cl(2p)_{1/2}$ and $Cl(2p)_{3/2}$ from $ZrCl(O_{\sim 0.43})$. Figure 13 shows the XPS of its O(1s). The shoulder at 529 eV is probably due to surface oxidation. Figure 14 shows the He I or UPS valence photoemission spectrum for both $ZrCl(O_{\sim 0.43})$ and ZrCl. The XPS valence spectrum of $ZrCl(O_{\sim 0.43})$ was washed out by the In backing because of the small amount of sample available.

The XPS of the Zr(3ds) and the UPS of $ZrCl(O_{\sim 0.43})$ were obtained immediately after the Ta tube was opened in the ESCA drybox. The rest were obtained six weeks later. In the meantime, the sample was stored in a sealed evacuated sample tube and only opened again to finish the data collection. The freshly prepared ZrCl was removed from its Ta tube in a drybox of lesser quality (~4 ppm H_2O and unknown O_2), sealed in a Ta tube, and then reopened only in the ESCA drybox prior to data collection.

A work function of 2.35 eV determined with the C(1s) and O(1s)[50] peaks was used to calculate the XPS binding energies (eV) of $ZrCl(O_{\sim 0.43})$: $Zr(3d)_{5/2}$, 179.9; $Zr(3d)_{3/2}$, 182.4; $Cl(2p)_{3/2}$,

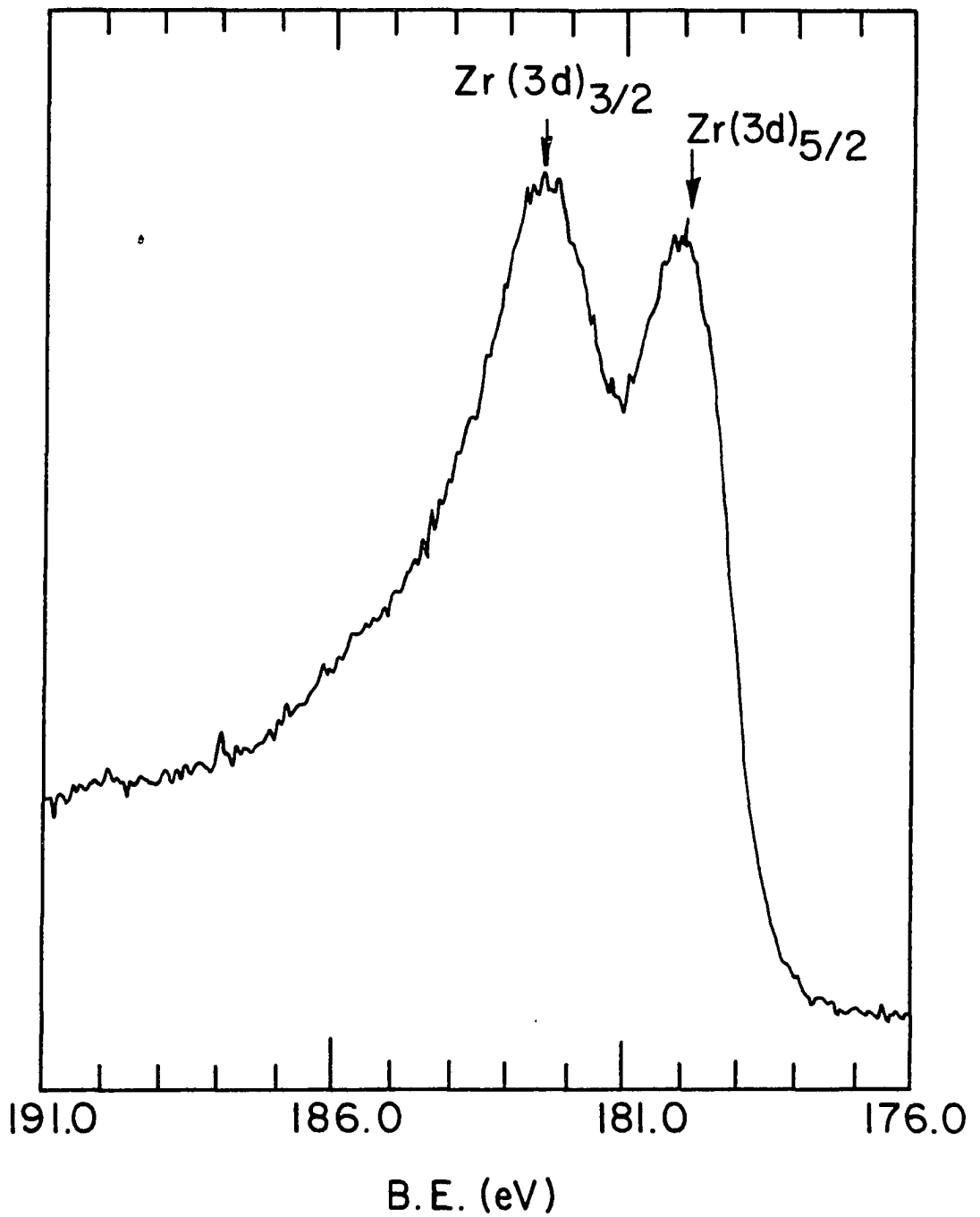

Figure 11. X-ray photoelectron spectrum for Zr(3d) from $ZrCl_{(0-0.43)}$. The ordinate scale is arbitrary

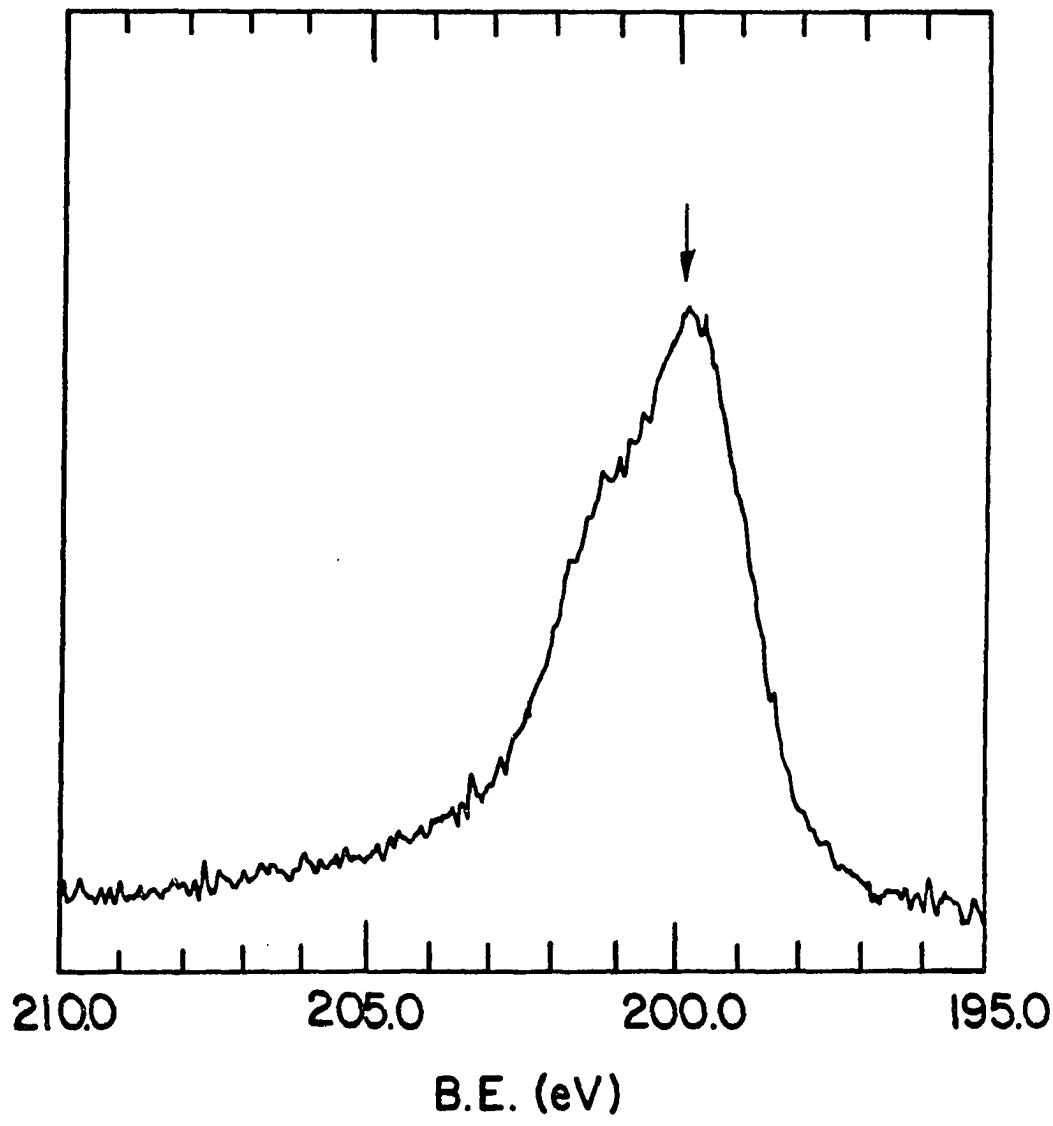

Figure 12. X-ray photoelectron spectrum for $Cl(2p)_{3/2}$(arrow) and $Cl(2p)_{1/2}$(shoulder) from $ZrCl(O_{\sim 0.43})$. The ordinate scale is arbitrary

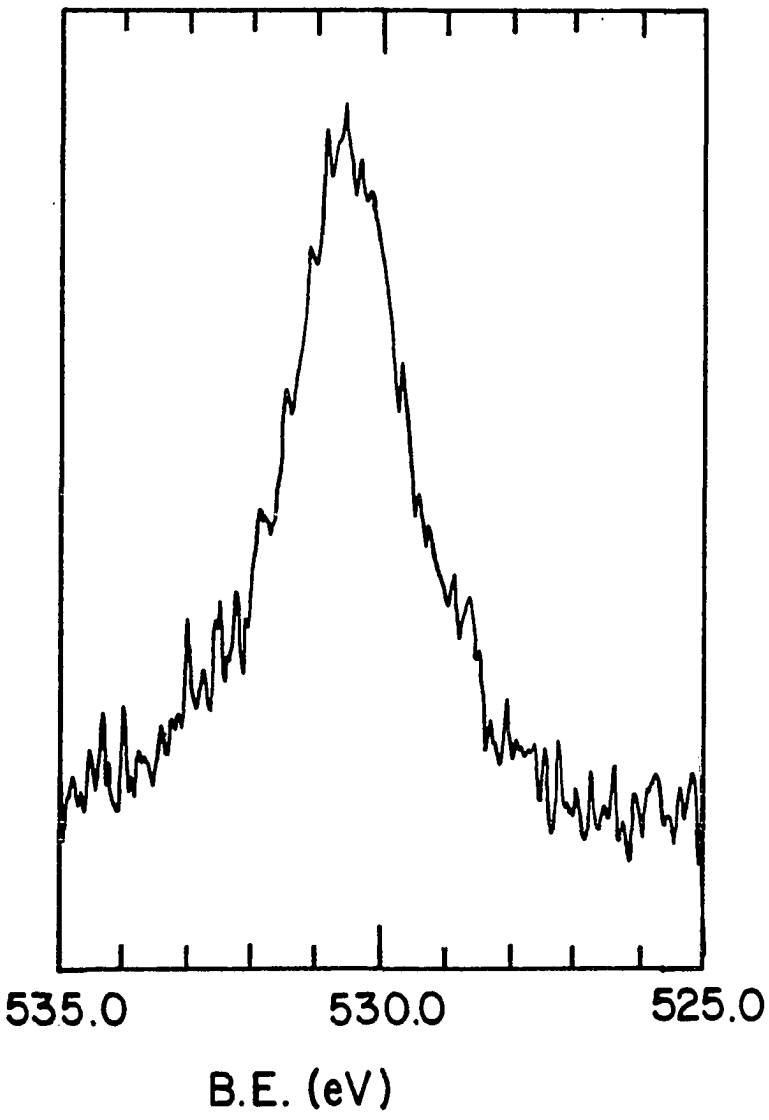

Figure 13. X-ray photoelectron spectrum for O(1s) from $ZrCl(O_{\sim 0.43})$. The ordinate scale is arbitrary

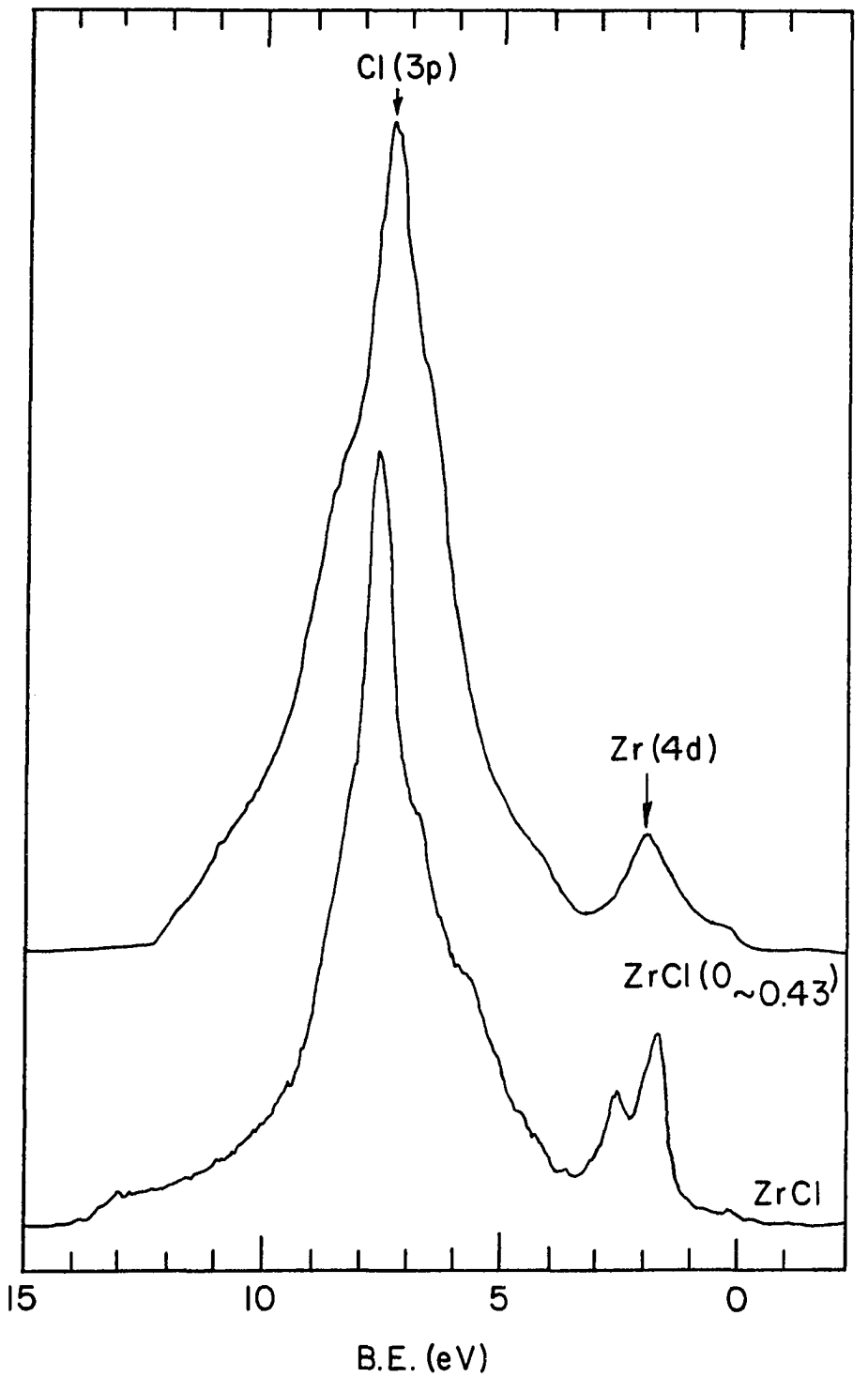

Figure 14. Valence region ultraviolet photoelectron spectrum for ZrCl and $ZrCl(O_{\sim 0.43})$. The ordinate scale is arbitrary

199.9; and O(1s), 530.6. The Zr(3d) peaks shifted to higher binding energies than found for ZrCl to approximately those of $ZrCl_{1.6}$, $ZrCl_{\sim 2.0}$, and Zr_6Cl_{12},[48] which have similar oxidation states for the metal. The Cl(2p) peak compares well with $ZrCl_{1.6}$, $ZrCl_{\sim 2.0}$, and Zr_6Cl_{12}.[48] The oxygen peak represents oxygen in a different environment than ZrO_2 because after some oxidation of the $ZrCl(O_{\sim 0.43})$, an additional oxygen peak, presumably from the ZrO_2 on the surface, appeared.

It is now believed after comparison with the UPS of $ZrCl(D_{0.5})$[49] that the E_F was misplaced in previous work[48,51] and should be as located in Figure 14, although only a weak Fermi edge at this point exists for ZrCl and $ZrCl(O_{\sim 0.43})$ and could be due to the In backing. ZrCl and $ZrCl(O_{\sim 0.43})$ show a mostly Cl(3p) at 7.6 and 7.3 eV, respectively, indicating a shift to lower binding energy for $ZrCl(O_{\sim 0.43})$. The shoulder on the high binding energy side of the Cl(3p) of $ZrCl(O_{\sim 0.43})$ is thought to be a result of oxygen. There are two peaks in the mostly Zr(4d) region for ZrCl at 1.7 and 2.5 eV, but there is only one for $ZrCl(O_{\sim 0.43})$ at 1.9 eV, a similarity it shares with the deuterides[49] and $ZrCl_2$.[51]

DISCUSSION

Intercalation

None of the intercalation attempts was clearly successful, while the same intercalate species have been easily incorporated into many dichalogenides. Corbett[52] recently pointed out electronic differences as a partial explanation of this. Intercalation involves essentially a direct coordination of a good base and thus reduction.[52] This requires an empty or partially filled metal band.[52] Those dichalogenides which possess this intercalate easily and those which don't, like MoS_2, intercalate only with great difficulty.[52] Although the band calculation of Marchiando et al.[9] indicated a substantial empty band just above the Fermi level, their electron-richness may be preventing additional coordination or reduction. Moving from d^3 to d^2, intercalation appears possible as recently seen for YX with K and Li.[31]

The reactive region of ZrX lies in the relatively electron-rich interstitial space between the metal layers. $ZrCl(H_y)$ was produced in the ammonia, pyridine and ethylenediamine attempts instead of species like $(NH_4^+)(ZrCl^-)$ with the cation between the chlorine layers (the van der Waals gap). The reason for this could be that the formation of ZrX(H) removes electrons from the system. Indeed, Liu (as cited in Reference 52) found the magnetic susceptibility of ZrCl increased slightly for $ZrClH_{0.5}$ and decreased for ZrClH and that this would be expected from density of state calculations which assume electron removal from the metal band.

Reaction of ZrX with ZrO_2

$ZrX(O_y)$ structure

The refinements (R values) for $ZrCl(O_y)$ improved with increased oxygen content (y). The z-coordinates (x and y fixed by symmetry) of Zr and Cl varied only slightly from ZrCl regardless of the amount of oxygen. As the amount of oxygen increased, the thermal parameters of the three structures became more nearly isotropic. This could be because the crystals became more perfect or the Zr_4O tetrahedron became more regular. The latter was, however, in all cases quite distorted with the intralayer and interlayer Zr-Zr distances different by ~0.3 Å which caused the tetrahedron to be flattened and forced the oxygen from the ideal position of 75% to 95% of the distance from the apex to the base. The oxygen position may have moved away from the Zr_4O base with increased oxygen content (Table 9), although the large uncertainties in the Zr_{apex}-O distances make this trend questionable.

Table 9 shows the a dimension increased significantly with the addition of oxide in ZrCl as a result of expansions in the intralayer Zr-Zr, Cl-Cl, and O-O distances. It is reasonable from a geometric standpoint that the addition of O would cause the Zrs, and thus the Cls, to spread apart within the layers. The c lattice dimension also increased significantly with the addition of oxide in ZrCl. Here the expansion occurred as a result of increases in the interlayer Zr-Zr, and Zr-Cl distances. The greater expansion between the Zr-Zr layers is reasonable from a geometric standpoint and from the removal of electrons which results in reduced metal-metal bonding. The smaller spread

between the Zr-Cl layers resulted from the Zr-O bonding competing with and weakening the Zr-Cl interactions. The Cl-Cl interlayer distance remained nearly constant, which is reasonable for a van der Waals gap. The O-O distances appeared to shrink although this trend is questionable because of their high uncertainties in $ZrCl(O_{0.25})$ and $ZrCl(O_{0.29})$ data. The higher uncertainties in the O-O distances are caused by a combination of the greater relative errors in the oxygen position and in the c dimension (relative to the a dimension). Since the angles were calculated from the bond distances, the errors accumulated again to yield high uncertainties in the interatomic angles which include the oxygen (Table 13). The trends in the various angles are a result of the expansions mentioned above and the position of the oxygen.

The refinement of the $ZrBr(O_y)$ structure could not identify the oxygen electron density presumed to be in the tetrahedral-like interstice between the Zr layers. This could be the result of the quality of the crystal but it gave very sharp spots as did every $ZrCl(O_y)$ crystal, or the quality of the diffractometer data but the agreement factor (R_{ave}, Table 1) was as good or better than those of the $ZrCl(O_y)$ data. This lack of oxygen position refinement could also be the result of the other atoms, Zr and Br, being so much heavier (better scatterers) and more abundant than the oxygen. In the $ZrCl(O_y)$ structures, the chloride and oxide both have low atomic weight compared with zirconium. The incorporation of a small amount of chloride in $ZrBr(O_y)$ could have contributed to the high R factor too.

As with the chloride structures, the Zr coordinate in ZrBr did not

change with the addition of oxide. The Br position did shift slightly but not significantly. The expansion in the a parameter again resulted from the increases in the intralayer Zr-Zr, O-O, and Cl-Cl distances. The c dimension expansion resulted from the increases in the interlayer Zr-Zr and Zr-Br distances. The relative increase in the interlayer Zr-Zr distance in $ZrBr(O_y)$ from ZrBr is less than observed with any of the monochloride oxide structures. This is because the interlayer Zr-Zr distance in ZrCl was shorter than in ZrBr to begin with but became about equal in their oxides at saturation. The relative increases in the Zr-X distance are about equal.

The X-ray crystal structure of the three stoichiometries of $ZrCl(O_y)$ could identify only one oxygen site with partial occupancy. The absence of a discernible supercell requires the oxygen to be disordered among the tetrahedral-like sites of which there is one per Zr. Thermodynamics as well as the interlayer O-O interactions presumably limit the oxygen occupation. Possibly shorter range ordering of oxygen occurs which is not discernible to X-rays.

It is interesting to compare the above with α-Zr which incorporates oxygen up to $Zr(O_{0.42})$[53] at 1000°, an almost identical O:Zr ratio as in the very different $ZrCl(O_{0.43})$. In the metal, however, the oxygens occupy octahedral sites. Interpretation of X-ray, electron, and neutron diffraction studies[54,55] has led researchers to believe several different orderings occur at different stoichiometry ranges. A solid solution exists up to $Zr(O_{0.25})$. Then in the approximate ranges of $Zr(O_{0.25})$-$Zr(O_{0.33})$, $Zr(O_{0.33})$, and $Zr(O_{>0.33})$, three different complex arrangements

of octahedral occupation exist. The unusual a and c parameter fluctuations with increasing oxygen content as seen in Figures 7 and 8 result. These orderings have been found with both annealing and rapid cooling. The cell dimensions of $ZrX(O_y)$, however, increase only linearly with increased oxygen content (Figures 1-4), suggesting only one kind of arrangement occurs.

The question arises as to why oxygen occupies the octahedral site in the metal but the tetrahedral-like site in ZrX. Table 16 compares, for the compounds concerned, the calculated sizes of the tetrahedral (-like) and octahedral (-like) holes determined from the distance from the appropriate metal to the interstitial equidistant point minus the Zr^{4+} (VI-coordinate) crystal radius of 0.86 Å reported by Shannon[56]. The crystal radius of O^{2-} (IV coordinate) is 1.26 Å. The tetrahedral sites in the metal are too small for oxygen occupation, but the octahedral

Table 16. Calculated sizes (Å) of tetrahedral (-like) and octahedral (-like) interstitials in various zirconium compounds

Compound	O occupation	T_d (-like)	O_h (-like)
Zr		1.07	1.41
$Zr(O_{0.43})$	Oh	1.09	1.42
ZrCl		1.15	1.45
$ZrCl(O_{0.43})$	Td	1.20	1.50
ZrBr		1.19	1.49
$ZrBr(O_{0.35})$	Td	1.21	1.50

sites are large enough. On the other hand, the tetrahedral-like sites of the ZrX structures are close in size to the oxide radius and would be expected to be preferred over the excessively large octahedral-like sites.

The sum of the crystal radii of Zr^{4+} and O^{2-} cited above is 2.10 Å. The Zr_{apex}-O and Zr_{base}-O distances in $ZrCl(O_{0.43})$ (Table 11) are 2.15(2) and 2.047(3) Å, respectively, which are only ±0.05 Å from this value. Furthermore, these distances compare well with other Zr-O distances found in the polymorphs of ZrO_2 and $Zr(O_{0.42})$ (Table 17).

The interlayer O-O distance at saturation ($ZrCl(O_{0.43})$) is 2.71(3) Å. In monoclinic ZrO_2, O-O distances range from 2.58(1) to 2.92 Å.[57] In tetragonal ZrO_2, each oxygen has two oxygen neighbors at 2.635 Å and four at 2.655 Å and is bonded to two zirconium atoms at 2.065 Å.[58] The $ZrCl(O_{0.43})$ O-O distance is certainly within the expected range.

Shannon[56] only reported a VI-coordinate S^{2-} radius of 1.70 Å, but the IV-coordinate radius would not be much greater. This is much too large to fit in even the octahedral-like interstice in ZrX. They reported the IV-coordinate F^- radius of 1.17 Å, which should fit in tetrahedral-like sites of ZrX but did not incorporate when ZrF_4 was used. Perhaps a different fluorinating agent would work. Shannon[56] reported the IV coordinate N^{3-} radius of 1.46 Å which should fit in the octahedral-like hole of ZrX but did not incorporate when ZrN was used. Perhaps a different nitriding agent would work. No crystal radius was reported for IV coordinate C^{4-} but it would be expected to be larger than N^{3-}, making it too large for either interstice. It did not

Table 17. Comparison of some Zr-O distances

Compound	d (Å)	Character
Cubic ZrO_2[a]	2.20	$CN[O^{2-}] = 4$ $CN[Zr^{4+}] = 8$
Tetragonal ZrO_2[b]	2.065 2.455	Flattened Td, $CN[O^{2-}] = 4$ Elongated Td, $CN[O^{2-}] = 4$ $CN[Zr^{4+}] = 8$
Monoclinic ZrO_2[c]	2.05 - 2.16 2.15 - 2.28	$CN[O^{2-}] = 3$ $CN[O^{2-}] = 4$ $CN[Zr^{4+}] = 7$
$Zr(O_{0.42})$	2.281	$CN[O^{2-}] = 6$ $CN[Zr] = 18$
$ZrCl(O_{0.43})$	2.047(3) Å 2.15(2)	Zr_{base}-O, $CN[O^{2-}] = 4$ Zr_{apex}-O, $CN[O^{2-}] = 4$ $CN[Zr] = 10$

[a]Reference 57.

[b]Reference 58.

[c]Reference 59.

incorporate when ZrC was used. The oxidation state of N^{3-} and especially C^{4-} may be unfavorable.

As mentioned in the introduction, the zirconium monohalide hydrides locate the hydride in the tetrahedral-like holes between the zirconium layers also. There are, however, several differences between the hydrides and oxides. The hydrides form as slightly nonstoichiometric (at elevated temperatures) hemi- and monohydrides[14] while the oxide continuously changes composition up to $ZrCl(O_{0.43})$. Furthermore, while there is no stacking order or symmetry change from ZrX to $ZrX(O_y)$, ZrXH has a one slab structure with space group $P\bar{3}m1$ and $ZrBrH_{0.5}$ has a single slab containing zig-zag chains of distorted tetrahedra with space group C2/m.[15] Also, the hydride in these structures is in ordered arrangements with all tetrahedral-like interstices occupied in the monohydride and alternate chains occupied in $ZrBrH_{0.5}$.[16]

The $ZrX(O_y)$ structure is closely related to the SmSI structure, which is a relatively uncommon trigonal analog to the very common tetragonal PbFCl structure. The SmSI structure differs from the $ZrX(O_y)$ structure in that the former has full chalogenide occupancy of the tetrahedral-like sites and no M-M bonding. β-ErOCl, TmOCl, YbOCl, and LuOCl are the only other oxychlorides known to have this structure type.[60] Interestingly, β-ErOCl transforms under high pressure to the PbFCl structure (α-ErOCl).[61] These rare earth oxychlorides form plates with graphitic character and have lattice dimensions analogous to $ZrX(O_y)$ but are red to white indicative of the higher oxidation states

of the metals.[62]

Corbett[63] classifies the Pauling bond order per electron pair (PBO/e) in the range >0.80 as indicative of very strong metal-metal bonding and 0.6-0.79 as indicative of moderate metal-metal bonding. The PBO/e for ZrCl of 0.82[63] drops to 0.78 for $ZrCl(O_{0.43})$. As is reasonable with oxidation, the Zr-Zr total bonding decreases but a little faster than appropriate as Zr-O bonding now also determines the layer separations. The bond order of $ZrCl(O_{0.43})$ is closer to that of ZrCl than $ZrCl_2$ (0.51)[63] and Zr_6Cl_{12} (0.68),[63] inconsistent with the photoelectron spectroscopy results which found the $Zr(3d)_{3/2}$, $Zr(3d)_{5/2}$, and Zr(4d) binding energies closer to those of $ZrCl_2$, Zr_6Cl_{12}, and $ZrCl_{1.6}$ than in ZrCl. The PBO/e for ZrBr is 0.66[63] and for $ZrBr(O_{0.29})$, 0.68. The initial matrix effects of substituting Br for Cl makes a large difference in the PBO/e but addition of oxide to the bromide makes practically no difference.

Zr coproduct

Even though attempts to measure halide in the Zr coproduct found very little there, the presence and type of halide appear to have an effect on the lattice dimensions (see General reactions section of RESULTS). Shannon[56] reported the VI coordinate crystal radii of Cl^- and Br^- as 1.67 and 1.82, respectively. Both appear too large for either interstice (Table 16).

The variable oxide content affects the a dimension similarly to

that with only oxide incorporation (Figure 5 vs. Figure 7). This and the appearance of the same superstructure line (d = 3.56 Å)[22] in both materials indicate that the same orderings of oxide occur in both cases. The various orderings of $Zr(O_x)$ described[54,55] require full availability beyond the third nearest neighbor octahedral hole and partial availability of the second nearest neighbor octahedral holes to oxide. Thus, the nearest neighbor octahedral hole to the oxide would be possible sites for X. This would also distribute the charge most equably and distort the lattice locally due to the large size of the halide compared to the size of the octahedral hole.

Reaction mechanism

The mechanism responsible for both transport and isothermal crystal growth near 1000° is not obvious and is still unknown. The Knudsen cell mass spectrometry experiment found mostly peaks from $ZrCl_4$. A small ClO^+ peak was found also, but the same peak was found to a lesser degree in $ZrCl_4$. This could be a fragment from Cl_2O or ClO_2, but no Cl_2O^+ or ClO_2^+ peaks were discovered. It is believed to be a result of the combination of oxygen in the vacuum line with fragmented Cl^+. If $ZrCl_4$ is a contributor to the transport, co-reaction with one or more vapor species which is reduced and contains oxygen is required. Since the pressure of $ZrCl_4$ is always very large, one cannot say much about its role anyway. The open Knudsen cell allowed such a rapid loss of $ZrCl_4$ that nothing else could be seen and the vapor pressures of the other species may be very small in comparison. Furthermore, the Knudsen cell

mass spectrometry experiment did not allow study under the closed system used in the isothermal and transport reactions.

The data for a and c lattice dimensions suggest the oxide does not evenly distribute between $ZrX(O_y)$ and Zr coproduct (Figures 1-8), but rather goes into the latter preferentially. This is supported by the results of the test of reversibility of oxide uptake where oxide was almost completely removed from $ZrCl(O_y)$ by added metal but $Zr(O_{0.3})$ remained, and the results of transport test of ZrCl alone where ZrCl was found together with $Zr(O_{0.10})$ at the hot end. At 850-1000°, oxygen diffuses quite rapidly in α-Zr at ~0.1-0.01 mm hr^{-1}.[64] Thus, the reaction mechanism could include oxygen incorporation via diffusion between contacting ZrO_2 particles and the Zr metal particles produced from disproportionation. The reactants were always ground together. Since structural and physical characteristics described in the introduction make ZrX essentially two-dimensional metals, it is possible that descent oxygen diffusion occurs within these double layers also. Thus, oxygen diffusion and vapor species reaction(s) in some combination should be considered in formulating the reaction mechanism.

Regardless of how the $ZrX(O_y)$ is formed, its transport capability is a potentially useful purification technique for Zr. Its selectivity for oxygen over other anions, as found with ZrN and ZrS, would make it useful to purify other materials were it not for the Zr metal which is the inevitable reduction product.

CONCLUSIONS AND FUTURE WORK

The present work provides additional basic information of oxygen presence between metal layers. The location of oxygen in the tetrahedral-like interstices in $ZrCl(O_y)$ vs. the octahedral-like interstices of ZrO_x for presumably size reasons provides an interesting and unique comparison. Such basic information is required for the eventual understanding of the factors responsible for the diffusion in and formation of oxygen superstructures (or the lack of them) in metals and metal compounds. This knowledge can be applied in a practical way to remedying the problem of the formation of a brittle oxidized zirconium layer which limits the temperature at which zirconium-based alloys can be used as cladding for nuclear fuel elements.

A major contribution of this work has been the discovery of the transport capability of $ZrX(O_y)$ in contrast to ZrX's lack of transport capability. This characteristic is potentially useful in the purification of Zr metal. Further investigations into the effects of the temperature gradients and heating period are needed. The former will require the use of a furnace with zone controls (Lindberg) and/or thermocouples in contact with the Ta tubing. Identification of the vapor species involved might be accomplished with Knudsen cell mass spectrometry with a super-small hole. The hole could possibly be made with a laser.

The $ZrCl(O_y)$ structure refinements could locate only one oxygen position, which requires disordered occupation of the tetrahedral-like

interstices between the Zr layers. However, as Yamaguchi[54] explains, it is difficult via X-ray diffraction to determine definitely the interstitial positions occupied by a small amount of oxygen in compounds with heavy atoms like Zr because of the comparatively weak scattering power of the oxygen atom. Neutron diffraction can be used to study the oxygen location more precisely because the thermal neutron coherent scattering amplitude of oxygen is almost comparable to that of zirconium (Zr, 0.62×10^{-12} cm; 0, 0.577×10^{-12} cm).[54] Electron diffraction on single crystalline specimens is particularly useful to detect the interstitial ordering when heavy metals are present because the interaction of electrons with crystals is $\sim 10^4$ times greater than that of X-rays.[54] For these reasons, neutron and electron diffraction studies should be undertaken to discern if there is some kind of ordered arrangement of the oxygens in $ZrCl(O_y)$. A large scale transport reaction could provide the samples necessary for neutron diffraction. A single crystal suitable for electron diffraction is more likely to be produced from a slowly cooled reaction.

Electron and neutron diffraction could also be used to examine orderings of oxide and possibly halide in the Zr coproduct. Comparison with the orderings found for $Zr(O_x)$ by Yamaguchi[54] and Fehlmann et al.[55] would be interesting. Transport reactions could provide the neutron diffraction samples. Electron diffraction data could be collected on single crystals obtained by cutting coarse grains from as-cast ingots as described by Yamaguchi[54] or thin foils as described by Fehlmann et al.[55] Zr metal and chloride impure ZrO_2 could be used to prepare the

as-cast ingots or thin foils.

The studies on ZrBr + n ZrO_2 found analogous results to those of ZrCl + n ZrO_2. The lower than expected lattice dimensions (Balanced equations section of RESULTS) and the inability of the $ZrBr(O_y)$ structure to satisfactorily refine (Structure results section of RESULTS), coupled with the small chloride impurity suggest that this work should be checked with chloride-free reactants. Photoelectron spectroscopy should be collected to compare other zirconium bromides.

The attempts to produce analogous phases to $ZrX(O_y)$ but with other anions instead of oxygen were unsuccessful. Further attempts to incorporate fluoride are especially worthwhile since its size is compatible with the ZrX tetrahedral-like holes. Perhaps NF_3 would work.

Unlike the rare earth halides (i.e., YCl, LaCl), there has been no evidence in this work or others of a MOX phase when M = Zr. The formation of $ZrX(O_y)$ and $Zr(O_x)$ must be responsible. Also, whereas intercalation attempts by this author and Daake[18] were unsuccessful, Ford[31] recently produced $K_{0.16}YClO_{0.82}$ via Y_2O_3 + Y + YCl_3 + 2 KCl at 950° for two weeks. YCl has the ZrBr structure.[65] In the compound above, oxide again incorporates into 82% of the tetrahedral-like interstices between the yttrium layers but potassium incorporates between the chloride layers. Interestingly, the interlayer O-O distances in $ZrCl(O_{0.43})$ and $K_{0.16}YClO_{0.82}$ are approximately equal ($ZrCl(O_{0.43})$, d_{O-O} = 2.71(3) Å; $K_{0.16}YClO_{0.82}$, 2.80(2) Å), but the latter has almost twice the amount of oxygen. Perhaps this distance limits the oxygen saturation. In any case, a similar attempt using ZrX + xs ZrO_2 + xs NaX

(LiCl, etc.) should be tried to produce an analogously intercalated $M_pZrX(O_y)$.

LITERATURE CITED

1. Struss, A. W.; Corbett, J. D. Inorg. Chem. 1970, 9, 1373.
2. Troyanov, S. I.; Tsirel'nikov, V. I. Russ. J. Inorg. Chem. (Engl.) Transl.) 1970, 15, 1762; Zh. Neorg. Khim. 1970, 15, 3379.
3. Dean, R. S. U.S. Patent 2 941 931, 1960.
4. Dean, R. S. Indust. Labs. 1959, 10, 45.
5. Troyanov, S. I.; Marek, G. S.; Tsirel'nikov, V. I. Russ. J. Inorg. Chem. (Engl. Transl.) 1973, 18, 135; Zh. Neorg. Khim. 1973, 18, 259.
6. Troyanov, S. I. Mos. Univ. Chem. Bull. (Engl. Transl.) 1973, 28, 89; Vestn. Mosk. Univ., Khim. 1973, 28, 369.
7. Adolphson, D. G.; Corbett, J. D. Inorg. Chem. 1976, 15, 1820.
8. Daake, R. L.; Corbett, J. D. Inorg. Chem. 1977, 16, 2029.
9. Marchiando, J. F.; Harmon, B. N.; Liu, S. H. Physica 1980, 99B, 259.
10. Daake, R. L.; Corbett, J. D. Inorg. Chem. 1978, 17, 1192.
11. Corbett, J. D.; Daake, R. L.; Cisar, A.; Guthrie, D. H. Electrochem. Soc. Symp. Proc. 1978, 78, 210.
12. Gamble, F. R. Science 1971, 174, 493.
13. Whittingham, M. S. Prog. Solid State Chem. 1978, 12, 41.
14. Struss, A. W.; Corbett, J. D. Inorg. Chem. 1977, 16, 360.
15. Marek, H. S.; Corbett, J. D.; Daake, R. L. J. Less-Comm. Met., in press.
16. Hwang, T. Y. et al. Phys. Lett. A 1978, 66A, 137.
17. Lapp, R. L.; Jacobson, R. A. Department of Chemistry, Iowa State University, unpublished research, 1979.
18. Daake, R. L. Ph.D. Dissertation, Iowa State University, Ames, Iowa, 1976.
19. Guthrie, D. H. Ph.D. Dissertation, Iowa State University, Ames, Iowa, 1981.

20. Corbett, J. D. Inorg. Syn. 1983, 22, in press.

21. "Selected Values of Chemical Thermodynamic Properties". Natl. Bur. Stand. (U.S.) Circ. 1971, Note 270-5.

22. Holmberg, B.; Dagerhamn, T. Acta Chem. Scand. 1961, 15, 919.

23. Schweiter, G. "Laboratory Report", Ames Laboratory, Iowa State University, Ames, Ia., 1978.

24. Fukutomi, M.; Corbett, J. D. J. Less-Comm. Met. 1977, 55, 125.

25. Conrad, B. R.; Franzen, H. F. High Temp. Sci. 1970, 3, 49.

26. Conrad, B. R.; Franzen, H. F. In "The Chemistry of Extended Defects in Non-Metallic Solids"; North Holland Publishing Company: Amsterdam, 1970; pp. 207-219.

27. Cisar, A. Ph.D. Dissertation, Iowa State University, Ames, Ia., 1978.

28. Araujo, R. E. M.S. Thesis, Iowa State University, Ames, Ia., 1981.

29. Yvon, K.; Jeitschko, W.; Parthé, E. "A Fortran IV Program for the Intensity Calculation of Powder Patterns", 1969 version; School of Metallurgy and Materials Science, Laboratory for Research on the Structure of Matter, University of Pennsylvania, Philadelphia, Pa., 1969.

30. Clark, C. M.; Smith, D. K.; Johnson, G. J. "A Fortran IV Program for Calculating X-ray Powder Diffraction Patterns--Version 5", Department of Geosciences, Pennsylvania State University, University Park, Pa., 1973.

31. Ford, J. E. Department of Chemistry, Iowa State University, personal communication, 1982.

32. Schroeder, D. R.; Jacobson, R. A. Inorg. Chem. 1973, 12, 210.

33. Jacobson, R. A. J. Appl. Crystallogr. 1976, 9, 115.

34. Rodgers, J.; Jacobson, R. A. Ames, Ia., 1967, AEC Report IS-2155.

35. Lawton, S. A.; Jacobson, R. A. Inorg. Chem. 1968, 7, 2124.

36. Scott, J. D. Department of Chemistry, Queens University, Kingston, Ontario, unpublished research, 1971.

37. Karcher, B. Ph.D. Dissertation, Iowa State University, Ames, Iowa, 1981.

38. "International Tables for X-ray Crystallography", Vol. III, 2nd ed.; Kynoch Press: Birmingham, England, 1962; p. 166.

39. Helland, B. Ames Laboratory, Iowa State University, unpublished research, 1981.

40. Powell, D. R.; Jacobson, R. A. Department of Chemistry, Iowa State University, unpublished research, 1979.

41. Johnson, C. K. "ORTEP: A Fortran Thermal-Ellipsoid Plot Program for Crystal Structure Illustrations", ORNL Report 3794, Oak Ridge National Laboratory, Oak Ridge, Tn., 1970.

42. Dines, M. B. Mat. Res. Bull. 1975, 10, 287.

43. Somoano, R. B.; Hodek, V.; Rembaum, A. J. Chem. Phys. 1973, 58, 697.

44. Ziebarth, R. L. Department of Chemistry, Iowa State University, personal communication, 1982.

45. Khodeev, Y. S.; Tsirel'nikov, V. I. Mos. Univ. Chem. Bull. (Engl. Transl.) 1973, 28, 82; Vestn. Mosk. Univ., Khim. 1973, 28, 611.

46. Domagala, R. F.; McPherson, D. J.; Hansen, M. Trans. AIME 1956, 206, 98.

47. Grozier, J. D. Pittsburgh, Pa., 1960, AEC Report WAPD-ZH-26.

48. Cisar, A.; Corbett, J. D.; Daake, R. L. Inorg. Chem. 1979, 18, 836.

49. Anderegg, J. W. Ames Laboratory, Iowa State University, personal communication, 1982.

50. Wagner, C. D.; Riggs, W. M.; Davis, L. E.; Moulder, J. F. "Handbook of X-ray Photoelectron Spectroscopy"; Muilenberg, G. E., Ed.; Perkin Elmer Corp.: Eden Prairie, Mn.

51. Corbett, J. D.; Anderegg, J. W. Inorg. Chem. 1980, 19, 3822.

52. Corbett, J. D. In "Intercalation Chemistry"; Whittingham, M. S.; Jacobson, A. J., Eds.; Academic Press: New York, 1982; Chapter 11.

53. Ackerman, R. J.; Garg, S. P.; Rauh, E. G. J. Am. Ceram. Soc. 1977, 60, 341.

54. Yamaguchi, S. J. Phys. Soc. Japan 1968, 24, 855.

55. Fehlmann, M.; Jostsons, A.; Napier, J. G. Kristallogr. 1969, 129, 318.

56. Shannon, R. D. Acta Crystallogr., Sect. A 1976, A32, 751.

57. Wells, A. F. "Structural Inorganic Chemistry", 4th ed.; Clarendon Press: Oxford, 1969; pp. 449.

58. Teuffer, G. Acta Crystallogr. 1962, 15, 1187.

59. Smith, D. K.; Newkirk, H. W. Acta Crystallogr. 1965, 18, 983.

60. Hulliger, F. In "Structural Chemistry of Layer-type Phases"; Lévy, F., Ed.; D. Reidel Publishing Company: Boston, 1976; Chapter IV, Section 14.

61. Beck, H. P. Z. Naturforsch. 1976, 31b, 1562.

62. Brandt, G.; Diehl, R. Mat. Res. Bull. 1974, 9, 411.

63. Corbett, J. D. J. Solid State Chem. 1981, 37, 335.

64. Douglas, D. L. "Metallurgy of Zirconium"; International Atomic Energy Agency. Vienna, 1971; pp. 287-289.

65. Mattausch, HJ.; Hendricks, J. B.; Eger, R.; Corbett, J. D.; Simon, A. Inorg. Chem. 1980, 19, 2128.

ACKNOWLEDGMENTS

The author would like to thank Professor J. D. Corbett for his help during the course of this work.

The help and cooperation of the past and present members of Physical and Inorganic Chemistry Group IX of the Ames Laboratory is very much appreciated.

F. Laabs, E. DeKalb, and J. Anderegg are thanked for their assistance in analyses.

Dr. R. A. Jacobson and the members of his group are thanked for their assistance in the crystallographic work.

The author would like to especially note the love, understanding, and sacrifices of her parents and family during her educational years. Special thanks are extended to Dr. John F. McClelland for his direction, encouragement, patience, and companionship during her graduate years.

APPENDIX A: OBSERVED AND CALCULATED STRUCTURE FACTORS (x10) FOR $ZrCl(O_{0.25(5)})$

H = 0

K	L	FO	FC
0	3	923	1006
0	6	867	708
0	9	925	721
0	12	1951	1799
0	15	1284	1119
0	18	1273	1038
0	21	1125	843
0	24	841	576
0	27	601	457
0	30	733	610
1	2	139	170
1	5	589	586
1	8	1927	1970
1	11	867	962
1	14	966	1113
1	17	7735	7624
1	20	863	825
1	23	509	565
1	26	677	759
1	29	727	838
2	1	669	685
2	4	1905	1892
2	7	682	642
2	10	817	702
2	13	697	625
2	16	1141	1035
2	19	626	621
2	22	813	767
2	25	789	751
3	0	1541	1454
3	3	520	482
3	6	340	343
3	9	438	426
3	12	1071	1058
3	15	576	557

H = 1

K	L	FO	FC
0	1	839	728
0	4	2486	2452
0	7	847	783
0	10	1094	921
0	13	837	1260
0	16	1231	1316
0	19	710	725
0	22	885	878
0	25	930	856
0	28	353	358
1	0	2345	2659
1	3	864	1078
1	6	541	539
1	9	696	714
1	12	1456	1434
1	15	791	741
1	18	808	829
1	21	808	829
1	24	471	502
1	27	362	408
2	2	59	117
2	5	408	434
2	8	1320	1348
2	11	565	580
2	14	615	690
2	17	490	562
2	20	561	634

H = 2

K	L	FO	FC
0	2	250	138
0	5	521	539
0	8	1722	1582
0	11	756	672
0	14	857	792
0	17	644	644
0	20	654	714
0	23	481	503
0	26	630	673
1	1	521	483
1	4	1561	1519
1	7	536	546
1	10	640	595
1	13	557	529
1	16	891	902
1	19	526	551
2	0	1286	1293
2	3	420	423
2	6	320	309

H = 3

K	L	FO	FC
0	3	552	482
0	6	359	343
0	9	455	426
0	12	1095	1058
0	15	580	557

APPENDIX B: OBSERVED AND CALCULATED STRUCTURE FACTORS (x10) FOR $ZrCl(O_{0.29(4)})$

H = 0

K	L	FO	FC
0	3	1055	1026
0	6	856	737
0	9	901	780
0	12	2120	1888
0	15	1116	1195
0	18	1136	1105
0	21	1000	970
0	24	698	676
0	27	547	536
0	30	645	697
1	2	139	145
1	5	574	558
1	8	2074	1965
1	11	922	998
1	14	1081	1120
1	17	822	784
1	20	877	856
1	23	613	612
1	26	849	826
1	29	964	969
2	1	616	677
2	4	1945	1833
2	7	659	608
2	10	794	720
2	13	705	641
2	16	1079	1031
2	19	632	618
2	22	859	834
2	25	841	858
3	0	1421	1375
3	3	497	465
3	6	305	325
3	9	415	421
3	12	1050	1027
3	15	573	561

H = 1

K	L	FO	FC
0	1	843	726
0	4	2571	2415
0	7	874	755
0	10	1105	963
0	13	936	1306
0	16	1397	1336
0	19	761	734
0	22	1011	980
0	25	1044	998
0	28	436	417
1	0	2233	2615
1	3	791	1069
1	6	527	543
1	9	689	745
1	12	1565	1461
1	15	851	778
1	18	851	856
1	21	778	807
1	24	547	578
1	27	446	465
2	2	74	94
2	5	403	394
2	8	1277	1276
2	11	561	572
2	14	651	660
2	17	556	554
2	20	596	624

H = 2

K	L	FO	FC
0	2	106	116
0	5	499	509
0	8	1613	1539
0	11	684	683
0	14	821	774
0	17	663	649
0	20	736	722
0	23	502	529
0	26	707	717
1	1	468	462
1	4	1455	1428
1	7	506	505
1	10	624	596
1	13	554	533
1	16	869	878
1	19	521	537
2	0	1164	1189
2	3	399	398
2	6	275	284

H = 3

K	L	FO	FC
0	3	482	465
0	6	340	325
0	9	433	421
0	12	1048	1027
0	15	582	561

APPENDIX C: OBSERVED AND CALCULATED STRUCTURE FACTOR (x10) FOR $ZrCl(O_{0.43(2)})$

H = 0

K	L	FO	FC
0	3	345	354
0	6	246	235
0	9	265	256
0	12	624	616
0	15	292	301
0	18	340	302
0	21	279	258
0	24	175	169
0	27	128	125
0	30	165	162
0	33	184	200
0	36	20	23
1	2	35	34
1	5	147	166
1	8	573	624
1	11	239	250
1	14	288	293
1	17	237	218
1	20	241	222
1	23	153	140
1	26	228	215
1	29	199	215
1	32	35	37
2	1	168	172
2	4	497	514
2	7	163	166
2	10	212	217
2	13	184	184
2	16	289	278
2	19	156	150
2	22	233	214
2	25	214	197
2	28	77	75
2	31	48	51
2	34	93	97
3	0	377	363
3	3	126	121
3	6	84	83
3	9	108	105
3	12	274	254
3	15	148	131
3	18	144	148
3	21	118	125
3	24	76	84
3	27	66	67
4	5	43	49
4	8	174	175
4	11	69	73
4	14	78	92

H = 1

K	L	FO	FC
0	1	217	240
0	4	673	768
0	7	205	228
0	10	298	315
0	13	248	255
0	16	372	371
0	19	206	192
0	22	291	272
0	25	266	249
0	28	96	95
0	31	57	62
0	34	107	119
0	37	151	166
1	0	636	646
1	3	214	221
1	6	141	141
1	9	183	186
1	12	421	424
1	15	208	214
1	18	243	230
1	21	209	197
1	24	133	131
1	27	99	100
1	30	136	131
1	33	156	162
2	2	23	22
2	5	105	101
2	8	346	336
2	11	148	140
2	14	177	172
2	17	135	129
2	20	154	138
2	23	95	92
2	26	138	139
2	29	142	140
3	1	76	77
3	4	261	247
3	7	89	80
3	10	104	107
3	13	88	87
3	16	138	141
3	19	80	79

H = 2

K	L	FO	FC
0	2	27	26
0	5	126	132
0	8	418	437
0	11	173	181
0	14	224	218
0	17	177	165
0	20	182	173
0	23	117	113
0	26	171	172
0	29	169	173
0	32	34	30
1	1	131	127
1	4	382	388
1	7	131	127
1	10	170	166
1	13	151	140
1	16	232	218
1	19	122	120
1	22	170	172
1	25	156	158
1	28	59	60
2	0	293	290
2	3	97	95
2	6	67	67
2	9	86	82
2	12	215	204
2	15	109	106
2	18	121	120
2	21	95	101

H = 3

K	L	FO	FC
0	3	122	121
0	6	87	83
0	9	107	105
0	12	257	254
0	15	133	131
0	18	150	148
0	21	125	125
0	24	79	84
0	27	67	67
1	2	19	15
1	5	60	61
1	8	227	215
1	11	86	90
1	14	106	113
1	17	81	83
1	20	88	89

H = 4

K	L	FO	FC
0	1	62	61
0	4	182	200
0	7	58	65
0	10	84	87
0	13	70	70

APPENDIX D: OBSERVED AND CALCULATED STRUCTURE FACTORS (x10) FOR $ZrBr(O_{0.29(6)})$

H = 0

K	L	FO	FC
0	3	617	599
0	6	1049	1193
0	9	382	295
0	12	2412	2270
0	15	2089	1790
0	18	1498	1465
0	21	639	592
0	24	452	303
0	27	1644	1454
0	30	376	330
0	33	1057	1190
1	2	1217	1180
1	5	2610	3059
1	8	478	412
1	11	995	847
1	14	139	160
1	17	1969	1920
1	20	858	888
1	23	1593	1354
1	26	453	328
1	29	475	416
1	32	843	1021
2	1	600	567
2	4	538	526
2	7	1293	1255
2	10	1767	1891
2	13	772	687
2	16	574	561
2	19	148	168
2	22	1316	1411
2	25	88	148
2	28	966	1114
3	0	1781	1655
3	3	261	200
3	6	487	483
3	9	176	174
3	12	1044	1038
3	15	859	873
3	18	598	743

H = 1

K	L	FO	FC
0	1	779	774
0	4	736	719
0	7	1600	1748
0	10	2264	2563
0	13	954	880
0	16	738	730
0	19	201	222
0	22	1760	1761
0	25	107	182
0	28	1462	1361
0	31	215	209
1	0	2652	2748
1	3	448	355
1	6	737	784
1	9	269	241
1	12	1743	1646
1	15	1495	1352
1	18	1098	1135
1	21	465	460
1	24	316	243
1	27	1145	1180
1	30	265	270
2	2	742	628
2	5	1827	1723
2	8	288	255
2	11	611	503
2	14	93	120
2	17	1238	1208
2	20	485	571
2	23	860	892
3	1	275	297
3	4	242	274
3	7	598	647

H = 2

K	L	FO	FC
0	2	939	819
0	5	2261	2205
0	8	349	317
0	11	758	635
0	14	108	141
0	17	1543	1499
0	20	668	704
0	23	1152	1092
0	26	299	270
1	1	496	453
1	4	435	417
1	7	1011	976
1	10	1453	1489
1	13	612	553
1	16	441	450
1	19	123	140
1	22	975	1152
2	0	1253	1345
2	3	179	165
2	6	335	393
2	9	133	142
2	12	786	851

H = 3

K	L	FO	FC
0	3	254	200
0	6	489	483
0	9	189	174
0	12	1057	1036
0	15	842	873
0	18	589	743
1	2	411	414
1	5	1072	1135